Electronic Supporting Information

Discovery and Evaluation of a Novel Selective Fluorescent Substrate for CYP3A4 Based on Sulfoxidation Characteristics

Chao-Hua Yan,†[a] Gui-Lin Wei,†[a] Zhuo-An Jin,†[a] Tian-Chi Lu,[a] Xiao-dong Li,[a] Ji-Cong Wu,[a] Chun-Yang Yu,[d] Li-Wei Zou,[a*] Ling Yang[ab*]

[a] Institute of Interdisciplinary Integrative Medicine Research, Shanghai University of Traditional Chinese Medicine, Shanghai, 201203, China

[b] Key Laboratory of Basic Pharmacology of Ministry of Education and Joint International Research Laboratory of Ethnomedicine of Ministry of Education, Zunyi Medical University, Zunyi, 563000, China

[c] School of Chemical Engineering, Ocean and Life Sciences, Dalian University of Technology, Panjin 124221, China

[d] School of Chemistry and Chemical Engineering, Frontiers Science Center for Transformative Molecules, Shanghai Jiao Tong University, Shanghai, 200240, China

†These authors (Chao-Hua Yan, Gui-Lin Wei and Zhuo-An Jin) contributed equally

E-mail: ylingdmpk1806@163.com (Ling Yang), chemzlw@163.com (Li-Wei Zou)

Table of contents

1. Synthesis and characterization of the probes

Reagents. NADPH, 1-aminobenzotriazole, sulfaphenazole, quinidine, clomethiazole, furafylline, resveratrol, sulfaphenazolum, clomethiazole, tranylcypromine, CYP3cide, omeprazole, ketoconazole, and montelukast were purchased from Med Chem Express (Shanghai) Ltd. All other reagents were of chromatographic grade or the highest commercially available purity. CYP1A1, CYP1A2, CYP2A6, CYP2A13, CYP2B6, CYP2C8, CYP2C9, CYP2C19, CYP2D6, CYP2E1, CYP2J2, CYP3A4, CYP3A5, and pooled human liver microsomes (HLM, n=50) were obtained from Research Institute for Liver Diseases (Shanghai) Co., Ltd. All microsomal samples and recombinant single enzymes were stored at −80 °C until use.

Instrumentation. Throughout the experiments, ultrapure water (18.2 MΩ) generated by a Millipore Direct-Q purification system was used. pH measurements were performed using a Leici PHB-4 pH meter (China). Absorption and emission spectra were measured using a spectrofluorophotometer (RF-5301pc, Japan). The NMR spectra (^{1}H at 400 MHz and ^{13}C at 100 MHz) of the compounds were recorded on a Bruker AVANCE III HD 400 MHz spectrometer (USA).

Analysis of NESF and NEUF was conducted using an LC-RF system (Shimadzu, Kyoto, Japan) equipped with a CBM-20A system controller, LC-20ADXR binary pumps, RF-20AXS fluorescence detector, SIL-20ACXR autosampler, Hypersil ODS C18 column (2.1×150 mm, 3 μm; Thermo), and an ODS guard column (2.1×150 mm, 3 μm; Thermo). The compounds were analyzed using a binary mobile phase consisting of 0.1% formic acid in water (B) and acetonitrile (A) with gradient elution at a flow rate of 0.4 mL/min. For LC-FD detection, the mobile phase consisted of (B) water containing 0.1% formic acid and (A) acetonitrile. The gradient elution program was as follows: 0-2.0 min, 95% B; 2-10 min, 95% B to 5% B; 10-12 min, 5% B; 12-15 min, re-equilibration to 95% B. The flow rate was maintained at 0.4 mL/min and the column temperature was kept at 40 ℃.

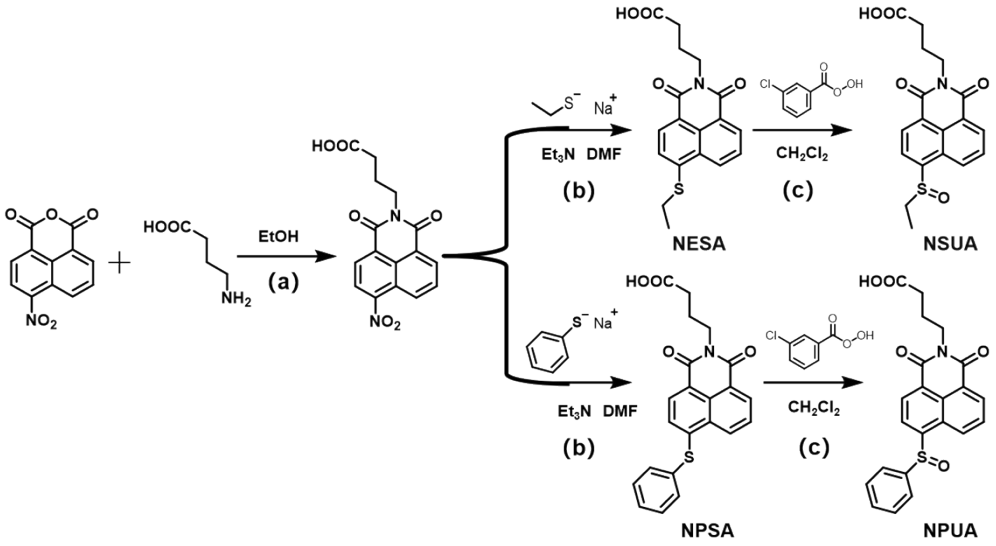

Scheme S1. Synthesis procedure of NESA, NPSA, and their sulfoxidation products.

Synthesis of NESA:

4-Nitro-1,8-naphthalic anhydride (1000 mg, 4.1 mmol) was dissolved in anhydrous ethanol, followed by the addition of 4-aminobutyric acid (466.5 mg, 4.5 mmol). The mixture was refluxed at 80 ℃ for 2 h. After cooling to room temperature, the reaction solution was poured into ice water, filtered, and washed with water to afford a light-yellow intermediate (1100 mg, yield: 74.5%). The intermediate (1100 mg, 3.35 mmol) was then dissolved in N, N-dimethylformamide (DMF), followed by sequential addition of triethylamine (553.7 μL, 3.35 mmol) and sodium ethanethiolate (845.6 mg, 10.05 mmol). The reaction proceeded at room temperature for 2 h (synthetic route shown in Scheme S1). Purification was performed via silica gel column chromatography (eluent: petroleum ether/ethyl acetate = 1:1 to remove impurities, followed by dichloromethane/methanol =5:1) to yield the target compound as a yellow solid (48.7% yield). The pure target compound **(NSUA)** was obtained as a white powdered solid (60.8% yield). **^{1}H NMR** (600 MHz, DMSO-d_6) δ 12.02 (s, 1H), 9.05 (d, J = 8.6 Hz, 1H), 8.66 (dd, J = 17.9, 7.5 Hz, 2H), 8.49 (d, J = 7.7 Hz, 1H), 8.10 (dd, J = 8.6, 7.3 Hz, 1H), 4.11 (t, J = 6.9 Hz, 2H), 3.57 (q, J = 7.3 Hz, 2H), 2.33 (t, J = 7.3 Hz, 2H), 1.92 (p, J = 7.1 Hz, 2H), 1.14 (t, J = 7.3 Hz, 3H). **^{13}C NMR** (151 MHz, DMSO-d_6) δ 174.53, 163.67, 163.19, 138.91, 131.68, 131.22, 130.57, 129.89, 129.69, 128.99, 127.99, 127.49, 123.84, 50.41, 31.74, 23.29, 7.56. **Q1MS-ESI** Calcd. For $[C_{18}H_{16}FNO_5S]^-$ ([M-H]$^-$), (m/z):342.09. Found 342.0.

Synthesis of NSUA:

NESA (20 mg, 0.058 mmol) was dissolved in dichloromethane, followed by the addition of 3-chloroperoxybenzoic acid (15 mg, 0.087 mmol). The reaction mixture was stirred at room temperature for 2 h (synthetic route shown in Scheme S1). Upon completion, the

mixture was extracted with dichloromethane and water. The organic phase was dried over anhydrous sodium sulfate and purified by silica gel column chromatography (eluent: dichloromethane/methanol = 20:1) to afford the target compound as a white solid (60.8% yield). The pure target compound **(NSUA)** was obtained as a white powdered solid (60.8% yield). **^{1}H NMR** (600 MHz, DMSO-d_6) δ 12.02 (s, 1H), 9.05 (d, J = 8.6 Hz, 1H), 8.66 (dd, J = 17.9, 7.5 Hz, 2H), 8.49 (d, J = 7.7 Hz, 1H), 8.10 (dd, J = 8.6, 7.3 Hz, 1H), 4.11 (t, J = 6.9 Hz, 2H), 3.57 (q, J = 7.3 Hz, 2H), 2.33 (t, J = 7.3 Hz, 2H), 1.92 (p, J = 7.1 Hz, 2H), 1.14 (t, J = 7.3 Hz, 3H). **^{13}C NMR** (151 MHz, DMSO-d_6) δ 174.53, 163.67, 163.19, 138.91, 131.68, 131.22, 130.57, 129.89, 129.69, 128.99, 127.99, 127.49, 123.84, 50.41, 31.74, 23.29, 7.56. **Q1MS-ESI** Calcd. For $[C_{18}H_{16}FNO_5S]^-$ ([M-H]$^-$), (m/z):358.08. Found 358.10.

Synthesis of NPSA:

4-Nitro-1,8-naphthalic anhydride (1000 mg, 4.1 mmol) was dissolved in anhydrous ethanol, followed by addition of 4-aminobutyric acid (466.5 mg, 4.5 mmol). The mixture was refluxed at 80 ℃ for 2 h. After completion, the reaction mixture was extracted with dichloromethane and water. The organic phase was dried over anhydrous sodium sulfate and purified by silica gel column chromatography (petroleum ether/ethyl acetate = 10:1) to afford the intermediate as a pale yellow solid (yield: 76.1%).The intermediate (328.3 mg, 1 mmol) was then dissolved in N,N-dimethylformamide (DMF), followed by sequential addition of triethylamine (165 μL, 0.26 mmol) and sodium benzenethiolate (396.48 mg, 0.78 mmol) (synthetic route shown in Scheme S1). Upon completion, the reaction mixture was extracted with dichloromethane and water. The organic phase was dried over anhydrous sodium sulfate and purified by silica gel column chromatography (initial elution with petroleum ether/ethyl acetate = 1:1 to remove impurities, followed by dichloromethane/methanol = 20:1) to yield the pure product as a yellow solid (56.2% yield). The pure target compound **(NPSA)** was obtained as a yellow powdered solid (56.2% yield). **^{1}H NMR** (600 MHz, DMSO-d_6) δ 12.04 (s, 1H), 8.63 (d, J = 8.3 Hz, 1H), 8.54 (d, J = 7.2 Hz, 1H), 8.32 (d, J = 7.8 Hz, 1H), 7.92 (t, J = 7.9 Hz, 1H), 7.59 – 7.48 (m, 5H), 7.37 (d, J = 7.8 Hz, 1H), 4.07 (t, J = 6.9 Hz, 2H), 2.30 (t, J = 7.3 Hz, 2H), 1.88 (t, J = 7.1 Hz, 2H). **^{13}C NMR** (151 MHz, DMSO-d_6) δ 174.46, 163.74, 163.59, 143.55, 133.89, 131.70, 131.15, 131.02, 130.77, 130.35, 129.38, 128.40, 128.20, 127.16, 123.39, 120.82, 31.76, 23.42, 11.27. **Q1MS-ESI** Calcd. For $[C_{22}H_{16}FNO_4S]^-$ ([M-H]$^-$), (m/z):390.0. Found 390.09.

Synthesis of NPUA:

NPSA (50 mg, 0.14 mmol) was dissolved in dichloromethane (DCM), followed by addition of 3-chloroperoxybenzoic acid (m-CPBA, 35.4 mg, 0.205 mmol). The reaction mixture was stirred at room temperature for 2 hours (synthetic route shown in Scheme S1). Upon completion, the mixture was extracted with dichloromethane and water. The organic phase was dried over anhydrous sodium sulfate and purified by silica gel column chromatography (eluent: petroleum ether/ethyl acetate = 1:1) to afford the product as a white solid (20 mg, 39.1% yield). The pure target compound **(NPUA)** was isolated as a white powdered solid (20 mg, 39.1% yield). **^{1}H NMR** (600 MHz, DMSO-d6) δ 8.97 (d, J = 8.7 Hz, 1H), 8.74 (d, J = 7.7 Hz, 1H), 8.67 (d, J = 7.8 Hz, 1H), 8.54 (d, J = 7.3 Hz, 1H), 8.08 (d, J = 7.4 Hz, 1H), 8.00 (dd, J = 8.7, 7.3 Hz, 1H), 7.91 – 7.90 (m, 1H), 7.71 (d, J = 2.1 Hz, 1H), 7.64 (d, J = 7.8 Hz, 1H), 7.54 (t, J = 8.1 Hz, 1H), 4.08 (t, J = 6.8 Hz, 2H), 2.30 (t, J = 7.3 Hz, 2H), 1.92 – 1.85 (m, 2H). **^{13}C NMR** (151 MHz, DMSO-d6) δ 166.58, 163.55, 163.05, 140.61, 134.79, 133.77, 133.07, 131.54, 131.09, 130.59, 130.39, 129.28, 128.99, 128.37, 128.22, 128.00, 126.59, 123.96, 31.67, 23.22. **Q1MS-ESI** Calcd. For $[C_{22}H_{16}FNO_5S]^-$ ([M-H] $^-$), (m/z): 406.08. Found 406.2.

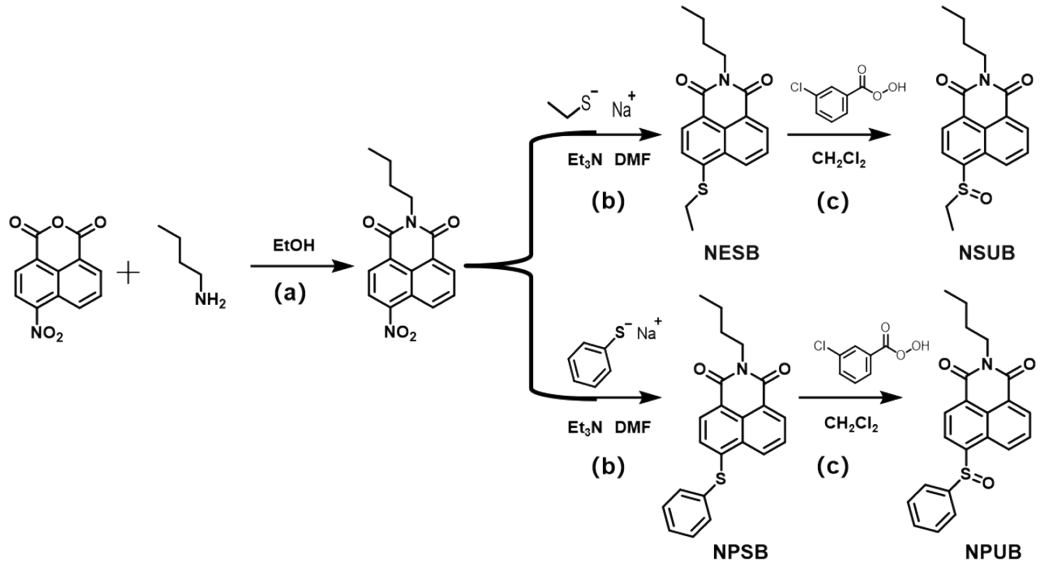

Scheme S2. Synthesis procedure of NESB, NPSB, and their sulfoxidation products.

Synthesis of NESB:

4-Nitro-1,8-naphthalic anhydride (121.6 mg, 0.5 mmol) was dissolved in anhydrous ethanol, followed by addition of n-butylamine (49.5 μL, 0.5 mmol). The mixture was refluxed at 80 ℃ for 2 h. After completion, the reaction mixture was extracted with dichloromethane and water. The organic phase was dried over anhydrous sodium sulfate and purified by silica gel column chromatography (petroleum ether/ethyl acetate = 10:1) to afford the intermediate

as a yellow solid (78 mg, 52.3% yield). The intermediate (78 mg, 0.26 mmol) was then dissolved in N, N-dimethylformamide (DMF), followed by sequential addition of triethylamine (65.6 μL, 0.26 mmol) and sodium ethanethiolate (43 mg, 0.78 mmol). The reaction proceeded at room temperature for 2h (synthetic route shown in Scheme S2). Purification was performed via silica gel column chromatography (eluent: petroleum ether/ethyl acetate = 5:1) to yield the product as a yellow solid (43.2% yield). The pure target compound **(NESB)** was obtained as a yellow powdered solid (43.2% yield). **^{1}H NMR** (600 MHz, DMSO-d_6) δ 8.51 (d, J = 7.8 Hz, 2H), 8.37 (d, J = 7.9 Hz, 1H), 7.87 (t, J = 7.9 Hz, 1H), 7.74 (d, J = 7.9 Hz, 1H), 4.03 (t, J = 7.5 Hz, 2H), 3.29 (t, J = 7.3 Hz, 2H), 1.64 – 1.59 (m, 2H), 1.40 (t, J = 7.3 Hz, 3H), 0.93 (t, J = 7.4 Hz, 3H).**^{13}C NMR** (101 MHz, DMSO-d_6) δ 163.64, 163.60, 144.97, 131.46, 130.92, 129.98, 129.07, 128.01, 127.60, 123.21, 123.16, 118.80, 30.17, 25.73, 20.31, 14.21, 13.91. **Q1MS-ESI** Calcd. For $[C_{18}H_{20}FNO_2S]^+$ ($[M+H]^+$), (m/z):314.11. Found 314.4.

Synthesis of NSUB:

NESB (35 mg, 0.11 mmol) was dissolved in dichloromethane (DCM), followed by addition of 3-chloroperoxybenzoic acid (m-CPBA, 29 mg, 0.17 mmol). The reaction mixture was stirred at room temperature for 2 hours (synthetic route shown in Scheme S2). Upon completion, the mixture was extracted with dichloromethane and water. The organic phase was dried over anhydrous sodium sulfate (Na_2SO_4) and purified by silica gel column chromatography (eluent: petroleum ether/ethyl acetate = 4:1) to afford the product as a white solid (20 mg, 55.6% yield). The pure target compound **(NSUB)** was obtained as a white powdered solid (20 mg, 55.6% yield). **^{1}H NMR** (600 MHz, DMSO-d_6) δ 9.05 (dd, J = 8.7, 1.1 Hz, 1H), 8.68 – 8.62 (m, 2H), 8.48 (d, J = 7.7 Hz, 1H), 8.10 (dd, J = 8.7, 7.3 Hz, 1H), 4.06 (t, J = 7.4 Hz, 2H), 3.57 (d, J = 7.4 Hz, 2H), 1.68 – 1.60 (m, 2H), 1.36 (dt, J = 14.7, 7.4 Hz, 2H), 1.13 (t, J = 7.3 Hz, 3H), 0.94 (t, J = 7.4 Hz, 3H). **^{13}C NMR** (101 MHz, DMSO-d_6) δ 163.47, 162.99, 138.92, 131.71, 131.24, 130.62, 129.90, 129.74, 129.28, 128.87, 127.83, 127.48, 123.70, 50.41, 29.97, 20.24, 14.18, 7.55. **Q1MS-ESI** Calcd. For $[C_{18}H_{20}FNO_3S]^+$ ($[M+H]^+$), (m/z):330.11. Found 330.2.

Synthesis of NPSB:

4-Nitro-1,8-naphthalic anhydride (1216 mg, 5.0 mmol) was dissolved in anhydrous ethanol, followed by addition of n-butylamine (495 μL, 5.0 mmol). The mixture was refluxed at 80 °C for 2 h. After completion, the reaction mixture was extracted with dichloromethane

and water. The organic phase was dried over anhydrous sodium sulfate and purified by silica gel column chromatography (petroleum ether/ethyl acetate = 10:1) to afford the intermediate as a yellow solid (780 mg, 52.3% yield). The intermediate (200 mg, 0.67 mmol) was then dissolved in N, N-dimethylformamide (DMF), followed by sequential addition of triethylamine (110.8 μL, 0.67 mmol) and sodium benzenethiolate (265.8 mg, 2.01 mmol). The reaction proceeded at room temperature for 2 h (synthetic route shown in Scheme S2). Upon completion, the mixture was extracted with dichloromethane and water. The organic phase was dried over anhydrous sodium sulfate and purified by silica gel column chromatography (petroleum ether/ethyl acetate = 4:1) to yield the product as a yellow solid (41.5% yield).The pure target compound **(NPSB)** was obtained as a yellow powdered solid (41.5% yield). **^{1}H NMR** (600 MHz, DMSO-d_6) δ 8.64 (dd, J = 8.4, 1.1 Hz, 1H), 8.54 (dd, J = 7.3, 1.1 Hz, 1H), 8.33 (d, J = 7.8 Hz, 1H), 7.92 (dd, J = 8.5, 7.3 Hz, 1H), 7.58 – 7.50 (m, 5H), 7.38 (d, J = 7.8 Hz, 1H), 4.05 – 4.00 (m, 2H), 1.64 – 1.58 (m, 2H), 1.39 – 1.31 (m, 2H), 0.92 (t, J = 7.4 Hz, 3H). **^{13}C NMR** (101 MHz, DMSO-d_6) δ 163.59, 163.44, 143.66, 133.92, 131.74, 131.12, 131.07, 130.78, 130.40, 129.83, 129.38, 128.33, 128.24, 127.15, 123.31, 120.72, 30.09, 20.26, 14.18. **Q1MS-ESI** Calcd. For $[C_{22}H_{20}FNO_3S]^+$ ($[M+H]^+$), (m/z):362.11. Found 362.4.

Synthesis of NPUB:

NPSB (40 mg, 0.11 mmol) was dissolved in anhydrous dichloromethane (DCM), followed by addition of 3-chloroperoxybenzoic acid (m-CPBA, 28.7 mg, 0.166 mmol). The reaction mixture was stirred at room temperature for 2 hours (synthetic route shown in Scheme S2). After completion, the mixture was extracted with dichloromethane and water. The organic phase was dried over anhydrous sodium sulfate (Na_2SO_4) and purified by silica gel column chromatography (eluent: petroleum ether/ethyl acetate = 1:1) to afford the pure target compound **(NPUB)** as a white solid (20 mg, 30.2% yield).The was obtained as a white powdered solid (20 mg, 30.2% yield). **^{1}H NMR** (600 MHz, DMSO-d_6) δ 8.75 – 8.66 (m, 2H), 8.53 – 8.48 (m, 2H), 7.93 (dd, J = 8.5, 7.3 Hz, 1H), 7.86 – 7.82 (m, 2H), 7.50 (d, J = 7.2 Hz, 3H), 4.02 (t, J = 7.4 Hz, 2H), 1.60 (p, J = 7.5 Hz, 2H), 1.34 (p, J = 7.5 Hz, 2H), 0.91 (t, J = 7.4 Hz, 3H). **^{13}C NMR** (101 MHz, DMSO-d_6) δ 166.55, 163.43, 163.25, 148.38, 144.90, 133.81, 133.18, 132.34, 131.58, 131.14, 130.73, 130.23, 129.29, 129.00, 128.94, 128.39, 128.24, 127.14, 125.84, 125.21, 123.73, 123.61, 29.99, 20.23, 14.17. **Q1MS-ESI** Calcd. For $[C_{22}H_{18}FNO_3S]^-$ ($[M-H]^+$), (m/z):376.11. Found 376.3.

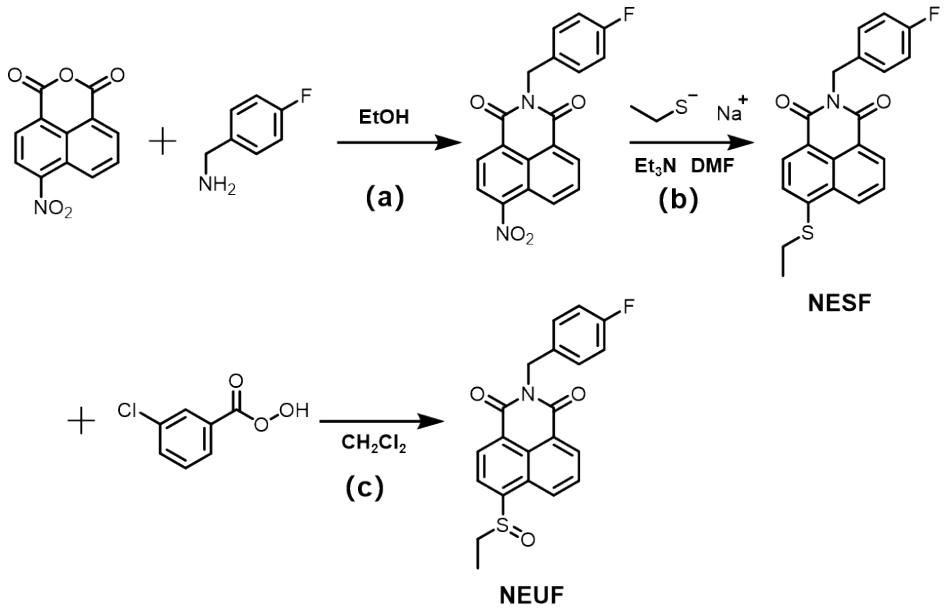

Scheme S3. Synthesis procedure of NESF, and their sulfoxidation products NEUF.

Synthesis of NESF:

4-Nitro-1,8-naphthalic anhydride (243.17 mg, 1 mmol) was dissolved in anhydrous ethanol, followed by addition of p-fluorobenzylamine (114 μL, 1 mmol). The mixture was refluxed at 80 ℃ for 2 h to afford a yellow intermediate (170 mg, 80% yield). After cooling to room temperature, the reaction mixture was poured into ice water, filtered, and washed with water to obtain the yellow intermediate (yield: 48.6%). The intermediate (170 mg, 0.485 mmol) was then dissolved in N, N-dimethylformamide (DMF), followed by sequential addition of triethylamine (80.2 μL, 0.485 mmol) and sodium ethanethiolate (122.5 mg, 1.456 mmol). The reaction proceeded at room temperature for 2 h (synthetic route shown in Scheme S3). Upon completion, the mixture was extracted with dichloromethane and water. The organic phase was dried over anhydrous sodium sulfate and purified by silica gel column chromatography (initial elution with petroleum ether/ethyl acetate = 4:1 to remove impurities, followed by petroleum ether/ethyl acetate = 1:1) to yield the product as a yellow solid (67.8% yield).The pure target compound **(NESF)** was obtained as a yellow powdered solid (67.8% yield). **^{1}H NMR** (600 MHz, Chloroform-d) δ 8.65 (dd, J = 7.3, 1.1 Hz, 1H), 8.58 (dd, J = 8.4, 1.2 Hz, 1H), 8.50 (d, J = 7.9 Hz, 1H), 7.76 (dd, J = 8.4, 7.3 Hz, 1H), 7.58 – 7.54 (m, 3H), 7.02 – 6.97 (m, 2H), 5.35 (s, 2H), 3.22 (q, J = 7.4 Hz, 2H), 1.50 (t, J = 7.4 Hz, 3H). **^{13}C NMR** (151 MHz, Chloroform-d) δ 164.09, 162.99, 161.36, 145.69, 133.19, 133.17, 131.78, 131.05, 130.96, 130.90, 130.32, 129.58, 128.41, 126.60, 123.02, 122.63, 118.90, 115.30, 115.15, 42.80, 26.37, 13.53. **Q1MS-ESI** Calcd. For $[C_{21}H_{17}FNO_2S]^+$ ($[M+H]^+$), (m/z):366.09. Found 366.0.

Synthesis of NEUF:

NESF (50 mg, 0.14 mmol) was dissolved in anhydrous dichloromethane (DCM), followed by addition of 3-chloroperoxybenzoic acid (mCPBA, 35.4 mg, 0.205 mmol). The reaction mixture was stirred at room temperature for 2 hours (synthetic route shown in Scheme S3). Upon completion, the mixture was extracted with dichloromethane and water. The organic phase was dried over anhydrous sodium sulfate (Na_2SO_4) and purified by silica gel column chromatography (eluent: petroleum ether/ethyl acetate = 1:1) to afford the product as a white solid (20 mg, 56.6% yield).The pure target compound **(NEUF)** was isolated as a white powdered solid. (20 mg, 56.6% yield). **^{1}H NMR** (600 MHz, Chloroform-d) δ 9.19 – 9.14 (m, 1H), 8.79 – 8.73 (m, 2H), 8.55 (d, J = 7.7 Hz, 1H), 7.98 (dd, J = 8.7, 7.3 Hz, 1H), 7.61 – 7.56 (m, 2H), 7.01 (t, J = 8.7 Hz, 2H), 5.37 (s, 2H), 3.35 (q, J = 7.4 Hz, 2H), 1.30 (t, J = 7.4 Hz, 3H).**^{13}C NMR** (151 MHz, Chloroform-d) δ 163.37, 163.15, 162.85, 161.52, 139.18, 132.22, 131.20, 131.15, 131.01, 130.51, 129.81, 129.31, 129.01, 127.88, 127.54, 123.42, 115.45, 115.31, 51.02, 43.16, 7.33.**Q1MS-ESI** Calcd. For $[C_{21}H_{15}FNO_3S]^-$ ([M-H]$^-$), (m/z):380.08. Found 380.3.

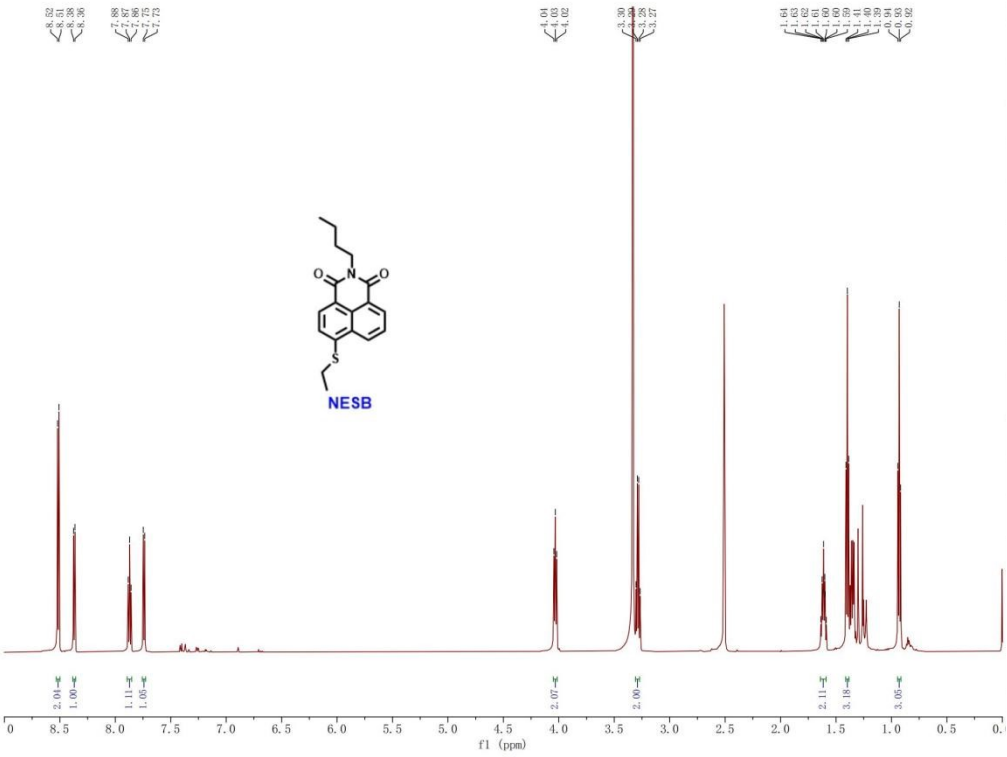

Fig. S1 ^{1}H NMR spectra of compound NESB in DMSO-d6.

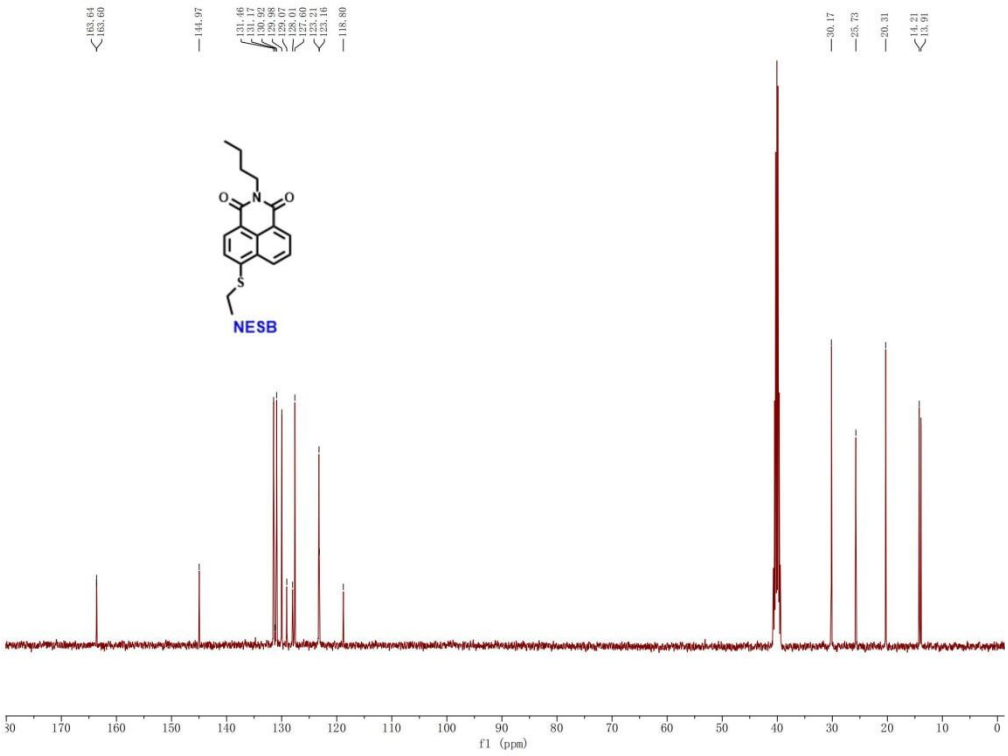

Fig. S2 ^{13}C NMR spectra of compound NESB in DMSO-d6.

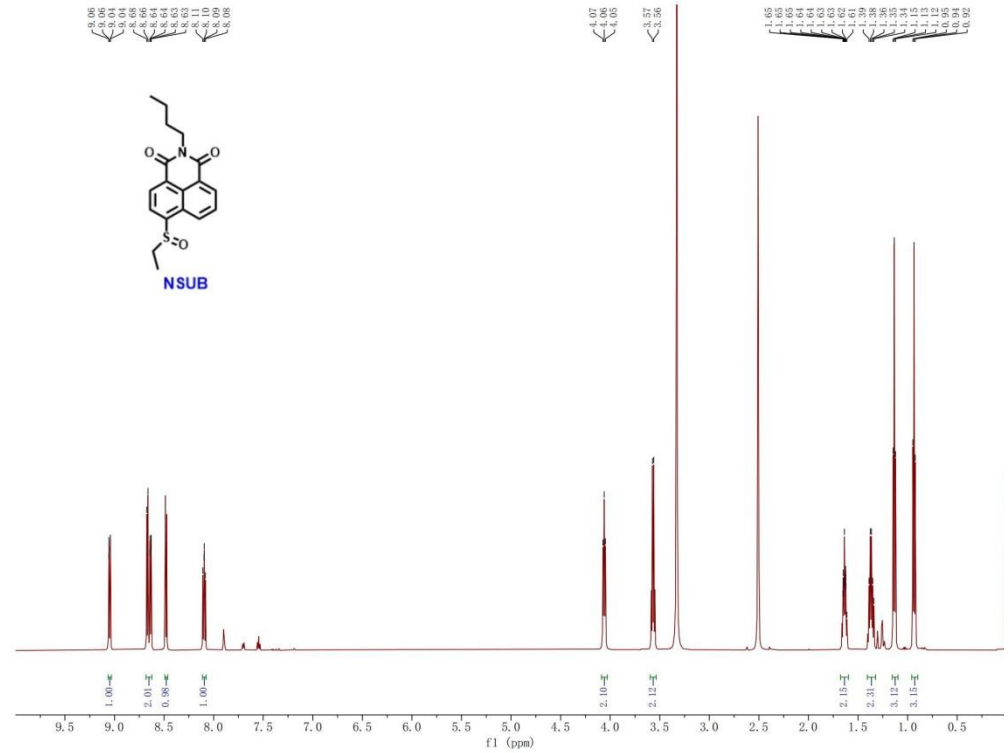

Fig. S3 ^{1}H NMR spectra of compound NSUB in DMSO-d6.

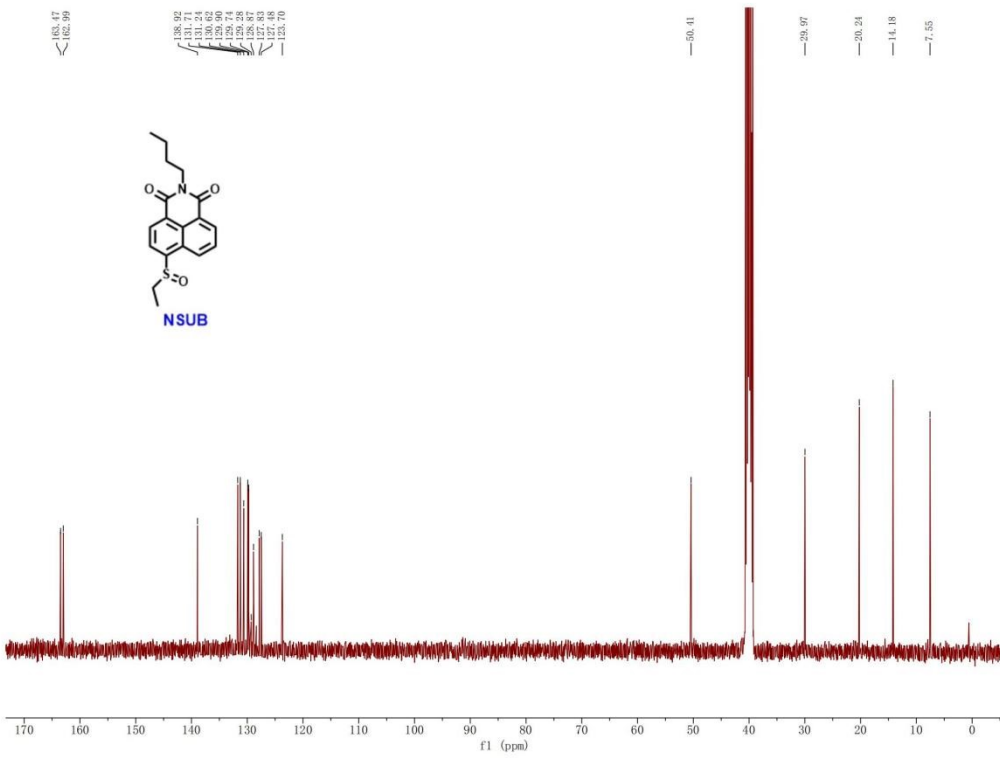

Fig. S4 ^{13}C NMR spectra of compound NSUB in DMSO-d6.

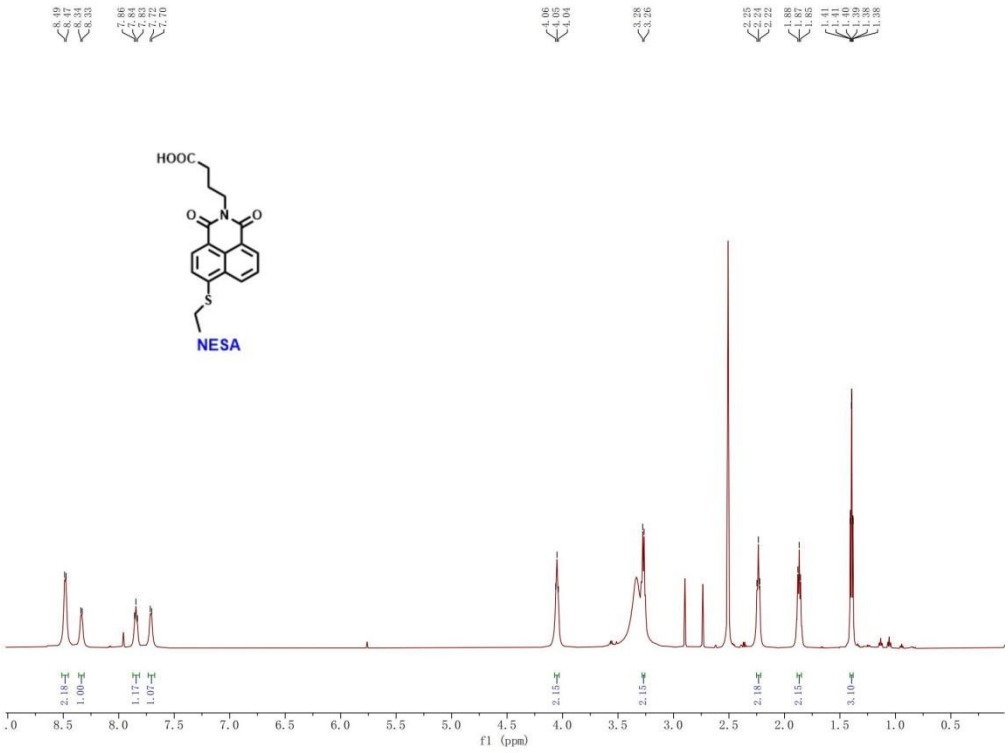

Fig. S5 ^{1}H NMR spectra of compound NESA in DMSO-d6.

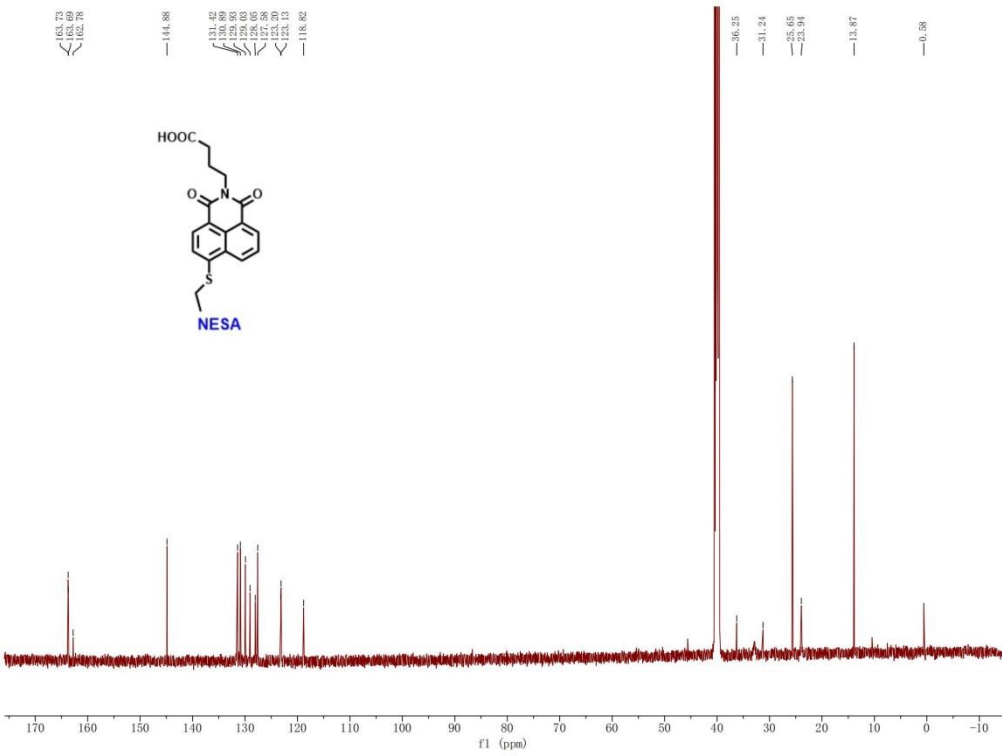

Fig. S6 ^{13}C NMR spectra of compound NESA in DMSO-d6.

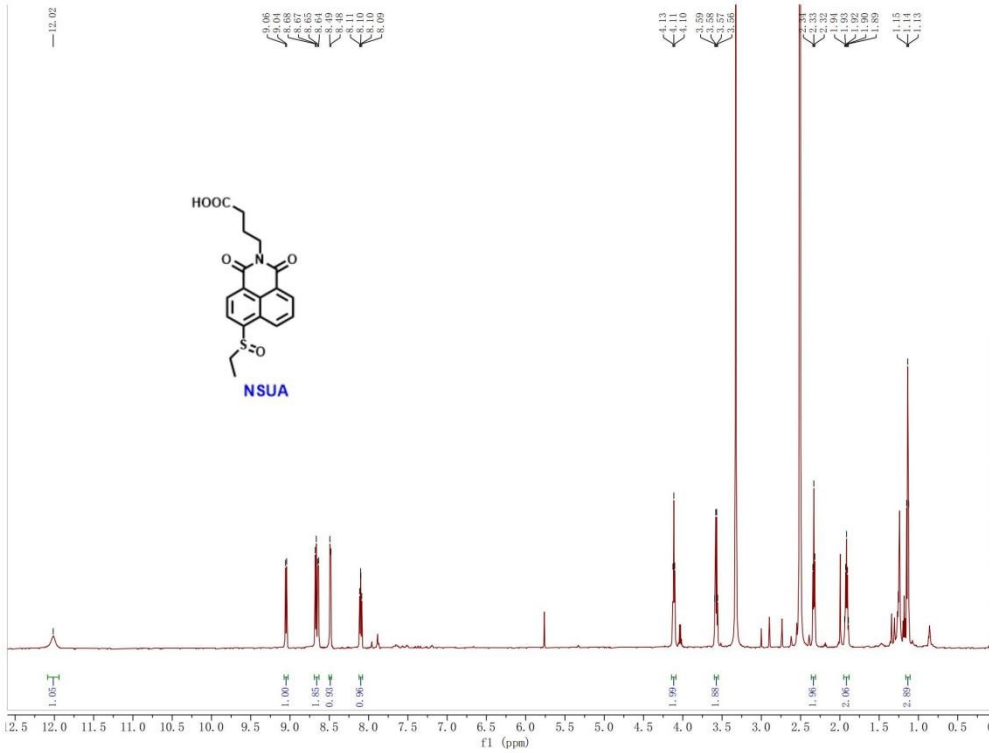

Fig. S7 ^{1}H NMR spectra of compound NSUA in DMSO-d6.

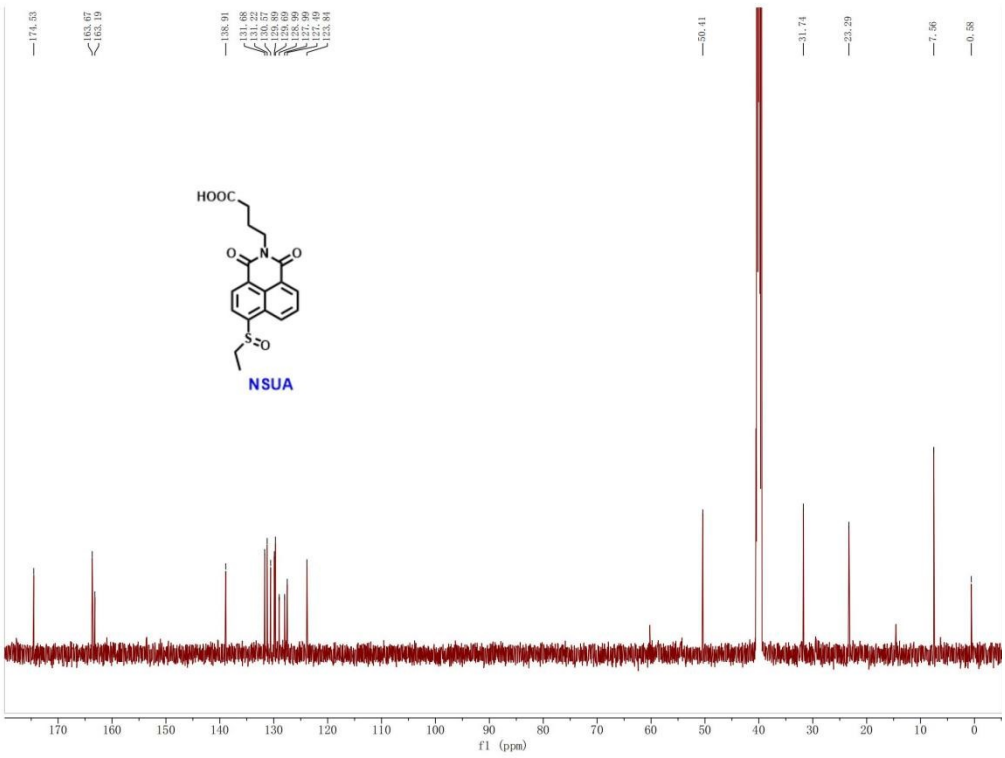

Fig. S8 ^{13}C NMR spectra of compound NSUA in DMSO-d6.

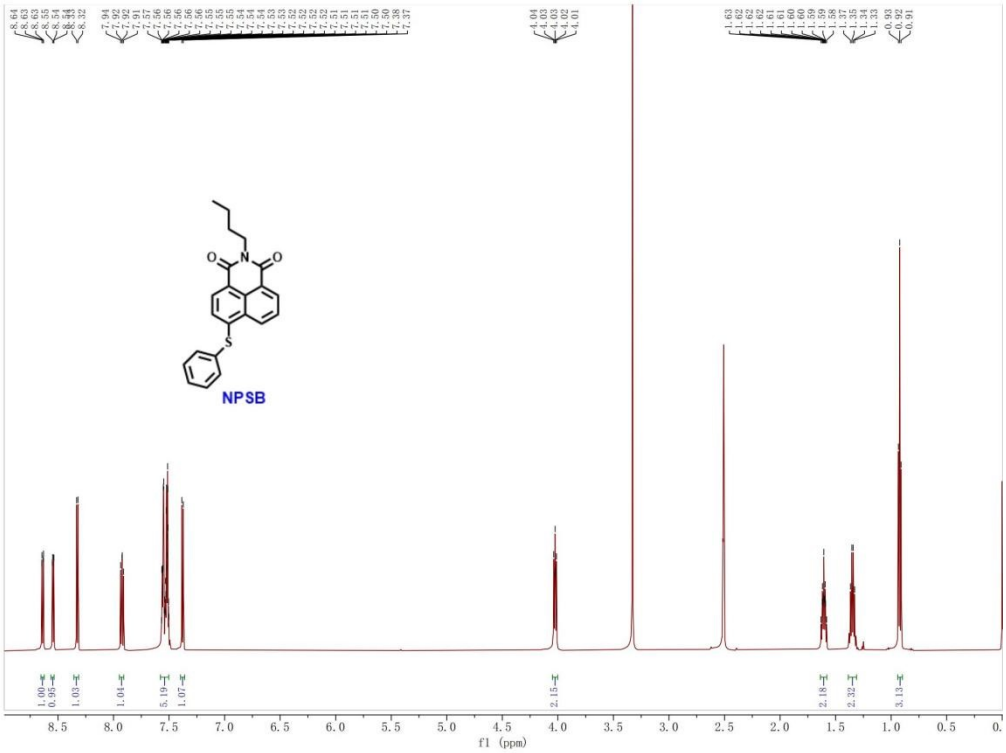

Fig. S9 ^{1}H NMR spectra of compound NPSB in DMSO-d6.

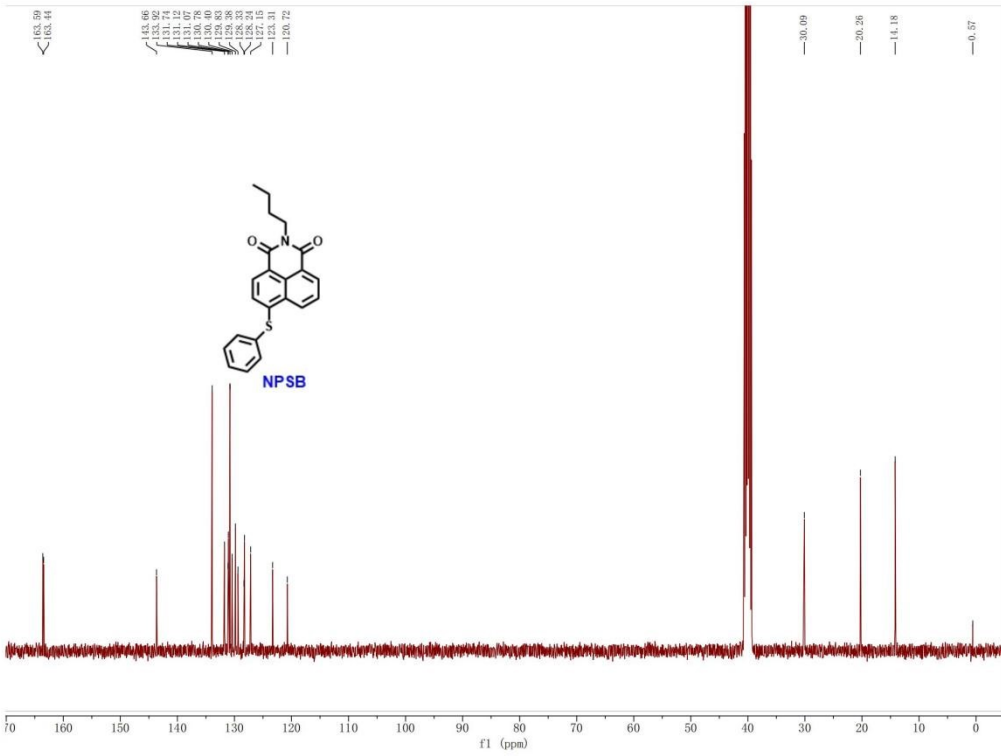

Fig. S10 ^{13}C NMR spectra of compound NPSB in DMSO-d6.

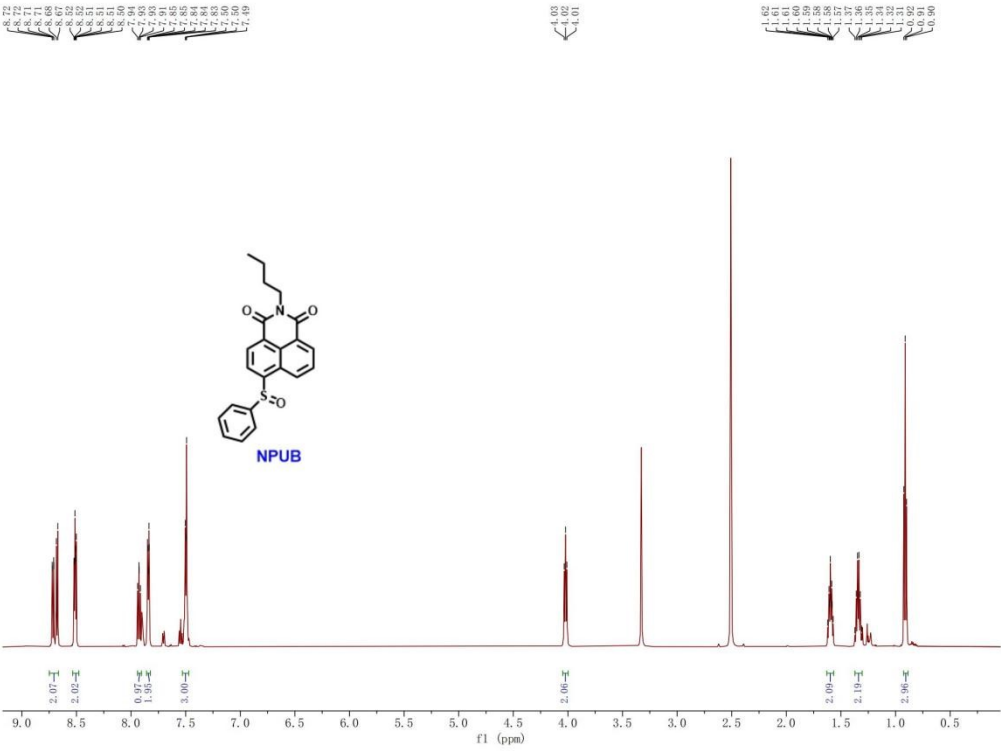

Fig. S11 ^{1}H NMR spectra of compound NPUB in DMSO-d6.

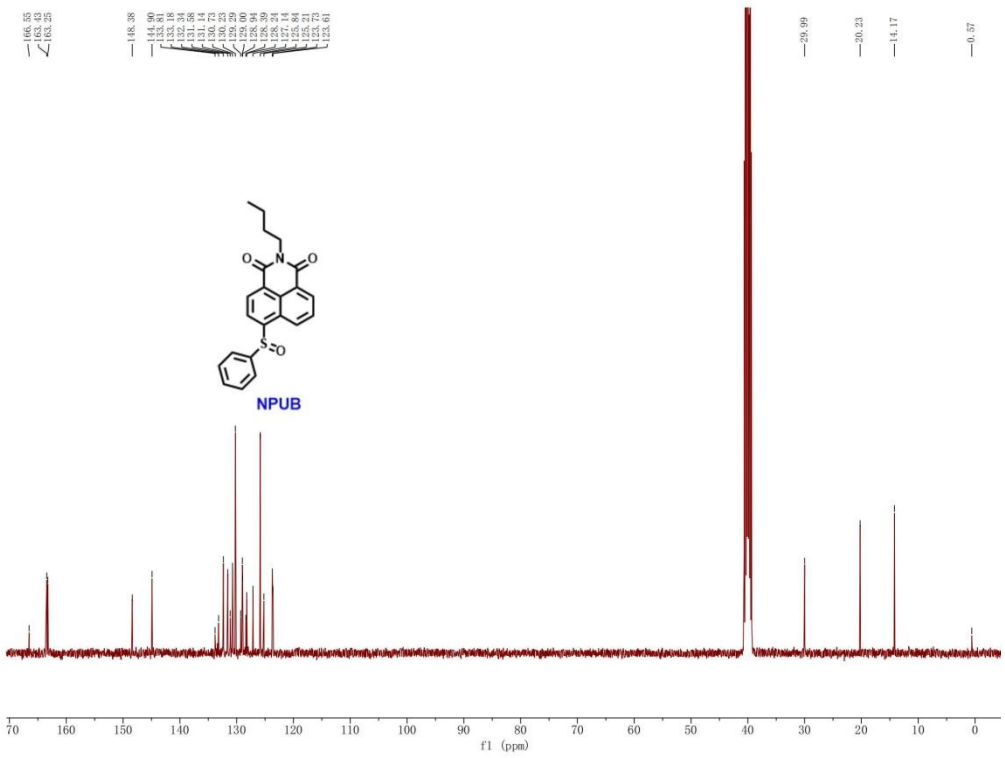

Fig. S12 ^{13}C NMR spectra of compound NPUB in DMSO-d6.

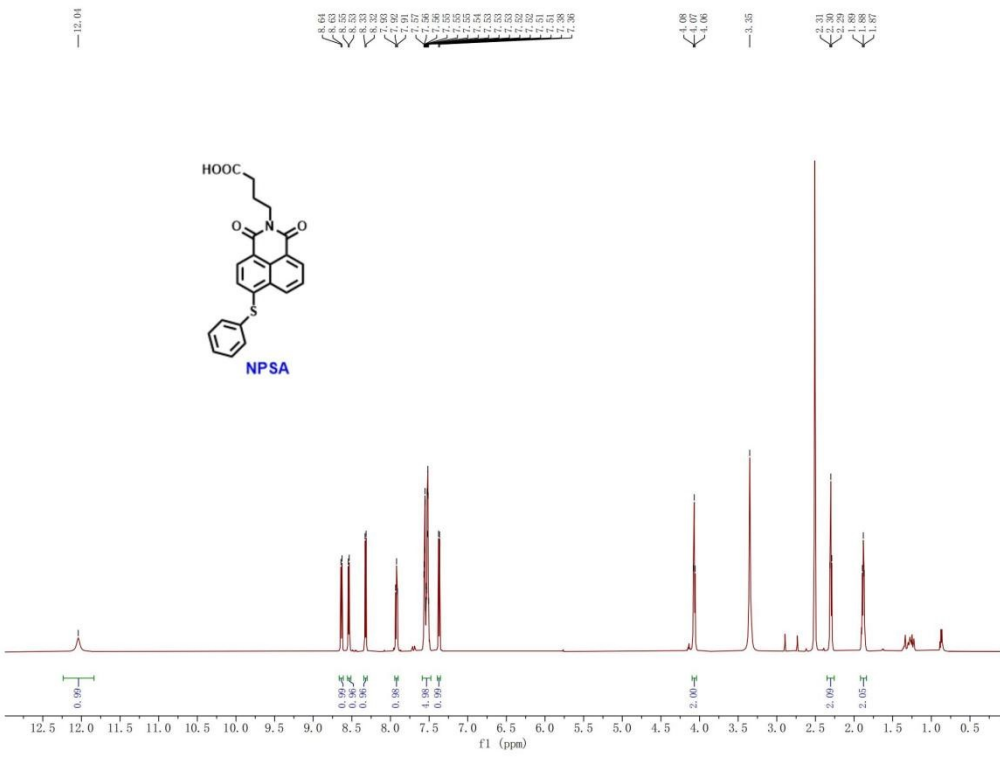

Fig. S13 ^{1}H NMR spectra of compound NPSA in DMSO-d6.

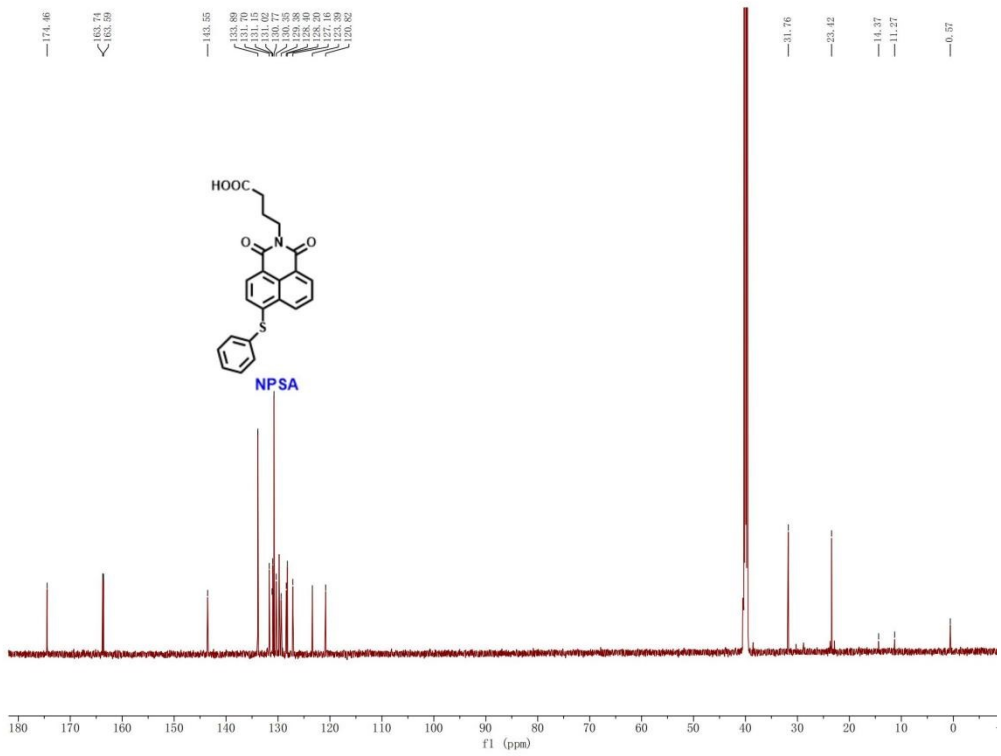

Fig. S14 ^{13}C NMR spectra of compound NPSA in DMSO-d6.

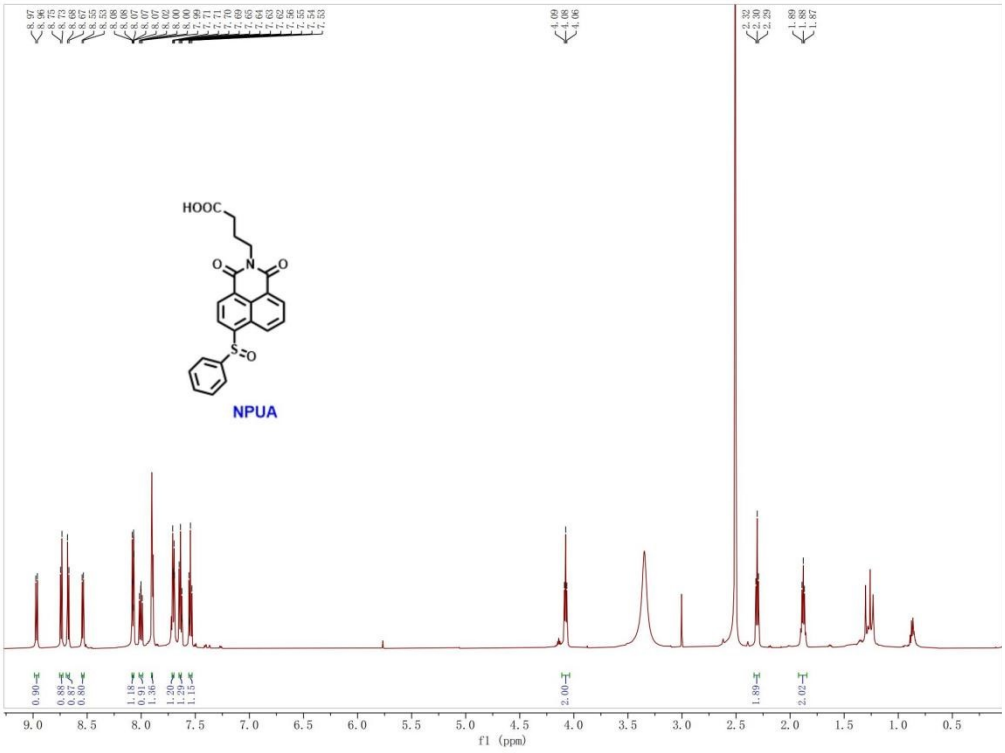

Fig. S15 ^{1}H NMR spectra of compound NPUA in DMSO-d6.

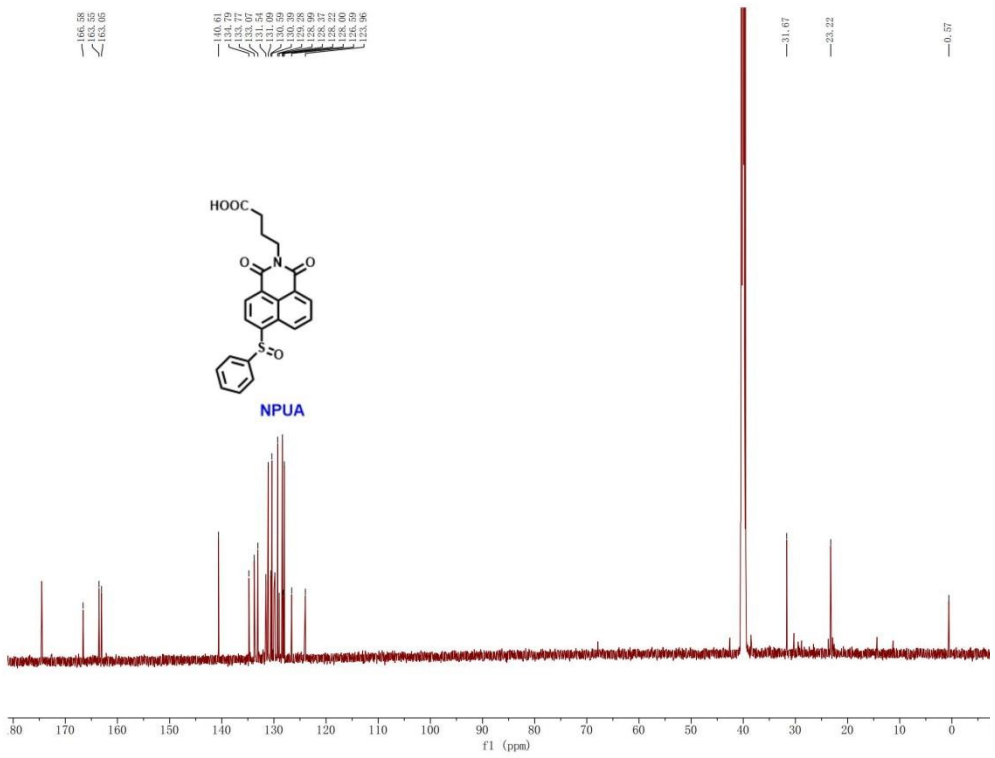

Fig. S16 ^{13}C NMR spectra of compound NPUA in DMSO-d6.

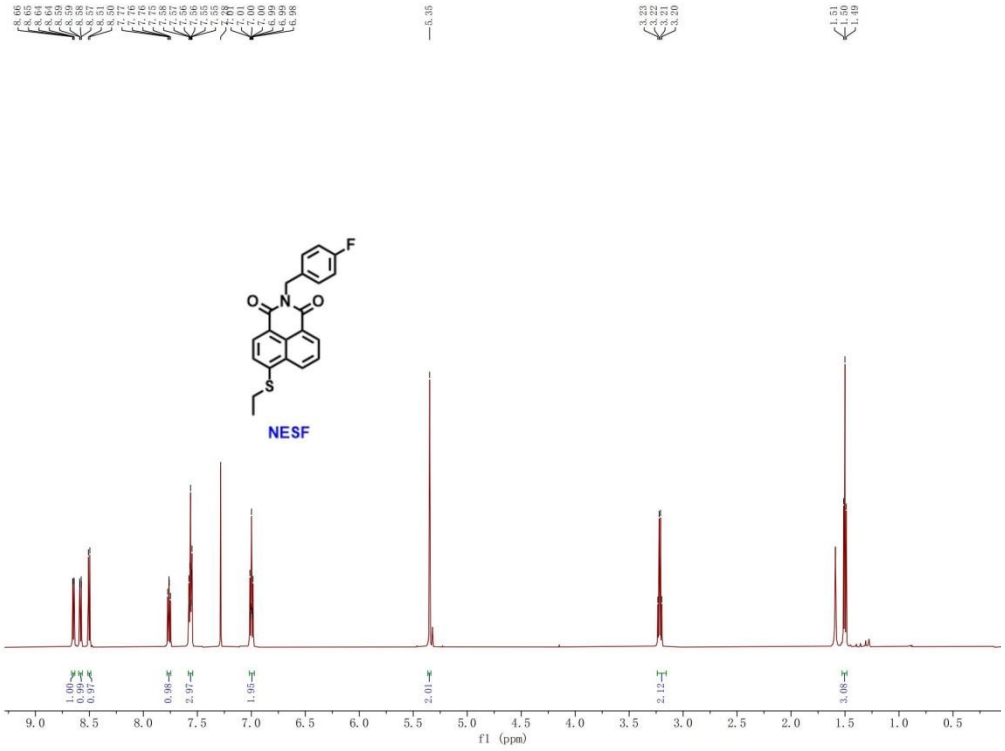

Fig. S17 ^{1}H NMR spectra of compound NESF in $CDCl_3$-d6.

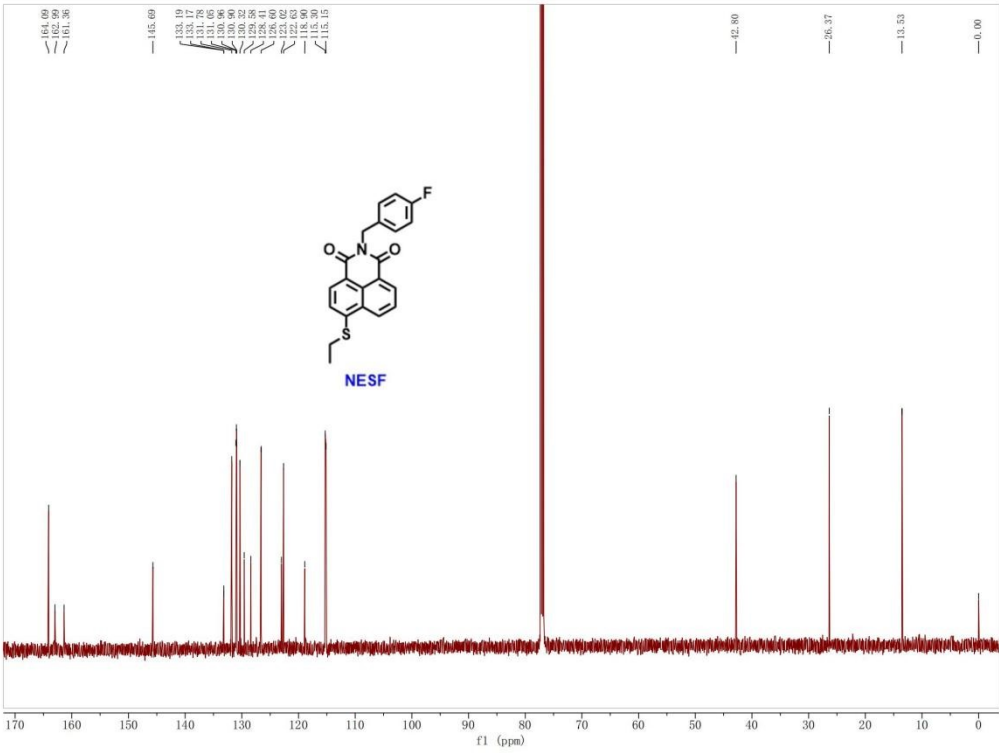

Fig. S18 ^{13}C NMR spectra of compound NESF in $CDCl_3$-d6.

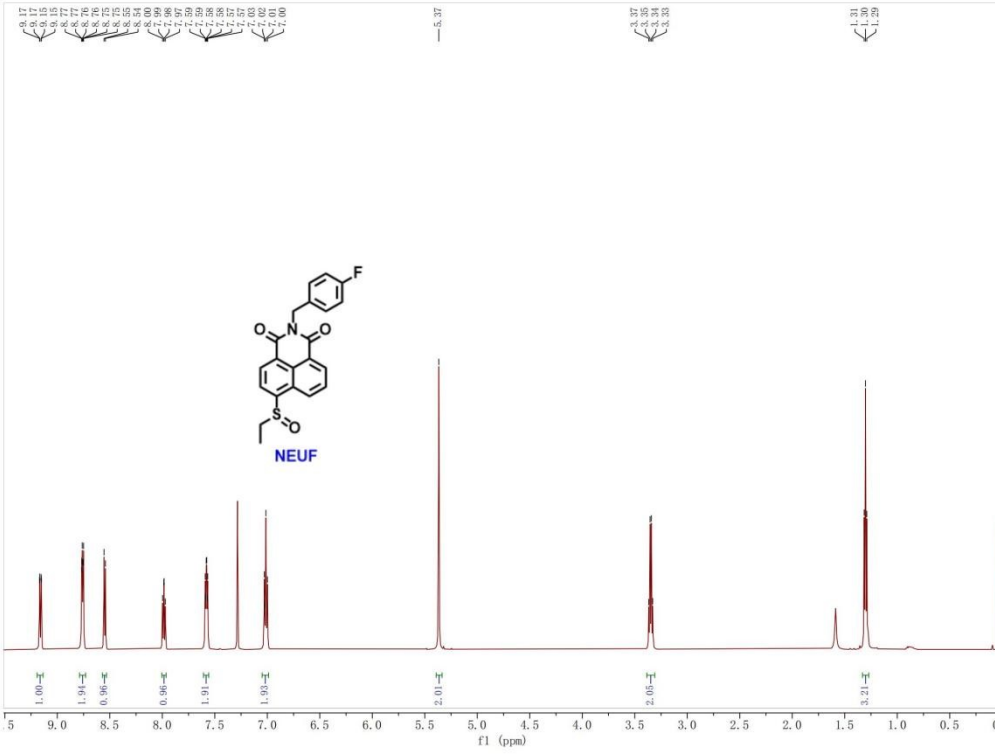

Fig. S19 ^{1}H NMR spectra of compound NEUF in $CDCl_3$-d6.

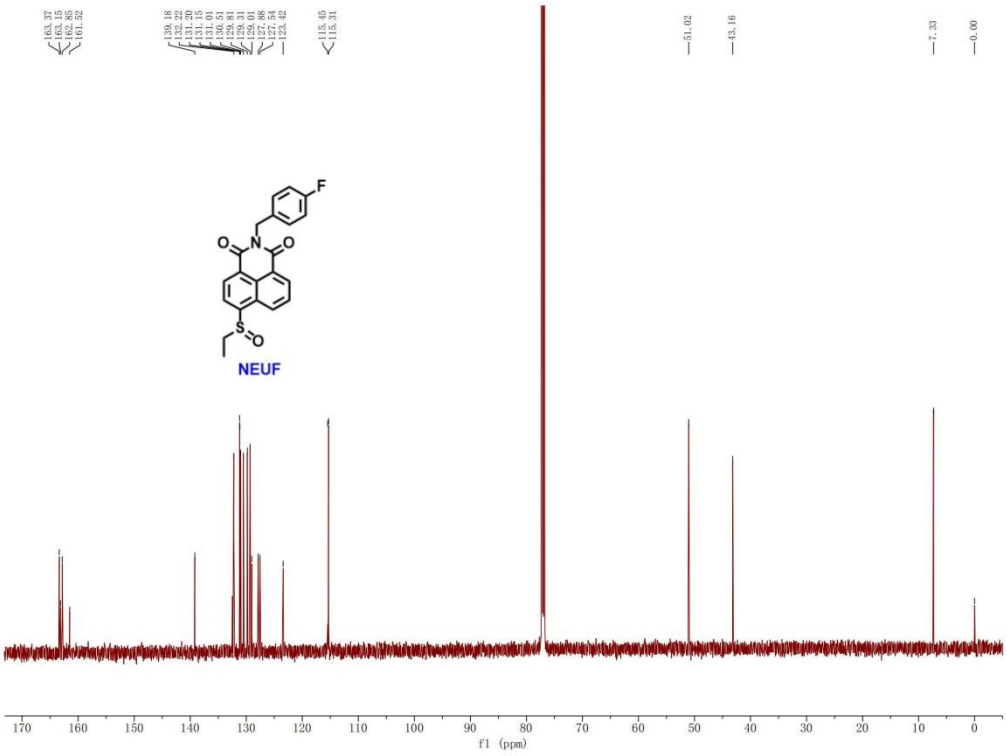

Fig. S20 ^{13}C NMR spectra of compound NEUF in $CDCl_3$-d6.

2.Recombinant single-enzyme assays and chemical inhibition experiments.

The synthesized compound NESF was systematically screened against 13 recombinant human cytochrome P450 isoforms (CYP1A1, CYP1A2, CYP2A6, CYP2A13, CYP2B6, CYP2C8, CYP2C9, CYP2C19, CYP2D6, CYP2E1, CYP2J2, CYP3A4, and CYP3A5) to evaluate its metabolic profile. In this assay, NESF was incubated with each individual CYP isoform (10 nM) in 100 mM phosphate-buffered saline (PBS, pH 7.4) with a final reaction volume of 200 μL. Following a 3-minute pre-incubation period at 37 ℃, the oxidative reactions were initiated by adding NADPH. The reaction mixtures were incubated at 37 ℃ for 60 minutes, with aliquots quenched every 15 seconds by adding 200 μL of ice-cold acetonitrile. All quenched samples were maintained on ice until completion of the time course, then centrifuged at 20,000×g for 20 minutes at 4 ℃. The resulting supernatants were carefully transferred to HPLC vials for subsequent analysis. Quantification of the metabolic product NEUF was performed by liquid chromatography with fluorescence detection (LC-FD) through measurement of peak areas. All experimental data were analyzed using GraphPad Prism software (version 9.5; GraphPad Software, Inc., La Jolla, CA, USA).

To further evaluate the inhibitory effects of CYP isoform-selective inhibitors on the sulfoxidation metabolism of NESF, we employed a panel of well-characterized P450 enzyme inhibitors:[1] ABT (a broad-spectrum CYP inhibitor), resveratrol (a known CYP1A1-specific

inhibitor), furafylline (a selective CYP1A2 inhibitor), tranylcypromine (a CYP2A6 inhibitor), montelukast (a reported CYP2C8 inhibitor), sulfaphenazole (a documented CYP2C9 inhibitor), omeprazole (a common CYP2C19 inhibitor), quinidine (a typical CYP2D6 inhibitor), clomethiazole (a potent CYP2E1 inhibitor), CYP3cide (a specific CYP3A4 inhibitor), and ketoconazole (an effective mammalian CYP3A inhibitor). The final concentrations of ABT, resveratrol, furafylline, tranylcypromine, montelukast, sulfaphenazole, omeprazole, quinidine, clomethiazole, CYP3cide, and ketoconazole were 500 μM, 100 μM, 10 μM, 2.5 μM, 10 μM, 10 μM, 10 μM, 10 μM, 5 μM, 1 μM, and 1 μM, respectively. Briefly, PBS, HLMs, substrate, and each CYP isoform-selective inhibitor/solvent were added to EP tubes, vortex-mixed, and pre-incubated at 37 ℃ for 3 minutes. Reactions were initiated by adding NADPH at 15-second intervals. After incubation at 37 ℃ for specified durations, reactions were terminated at 15-second intervals by adding 200 μL of ice-cold acetonitrile. All quenched samples were maintained on ice until completion of the time course, then centrifuged at 20,000×g for 20 minutes at 4 ℃. The supernatants were transferred to HPLC vials, and the product formation rates were quantified by LC-FD in both the presence and absence of inhibitors. All data were analyzed using GraphPad Prism software (version 9.5; GraphPad Software, Inc., La Jolla, CA, USA).

3.Enzymatic Kinetic Analysis

We investigated the metabolic kinetics of NESF using both recombinant human CYP3A4 and human liver microsomes (HLM). The incubation system (200 μL total volume) contained PBS buffer (100 mM, pH 7.4), NESF (0-30 μM), NADPH, and either 0.1 nM CYP3A4 or 0.2 mg/mL HLM. Briefly, PBS, substrate, and CYP3A4/HLM were combined in 1.5 mL EP tubes, vortex-mixed, and pre-incubated at 37 ℃ for 3 min. Reactions were initiated at 15-second intervals by adding NADPH. After 60 min incubation at 37 ℃, reactions were terminated with 200 μL ice-cold acetonitrile. All quenched samples were centrifuged at 20,000×g for 20 min at 4 ℃, and the supernatants were transferred to HPLC vials for LC-FD analysis. Enzyme kinetic curves were fitted using GraphPad Prism 9.5.

4.Method Validation

We established an LC-FD analytical method and validated its accuracy for NESF and NEUF analysis. First, we analyzed three types of samples by LC-FD: NESF standard solution (20 μM), NEUF standard solution (20 μM), and NESF co-incubated with HLM (precipitated with acetonitrile and centrifuged). After confirming NEUF formation from NESF metabolism in HLM incubations, we developed calibration curves for both compounds and determined the limit of detection (LOD) and limit of quantification (LOQ) for NEUF. We evaluated precision,

accuracy, intra-batch variation and inter-batch variation. For intra-batch assessment, we performed triplicate measurements of NESF and NEUF samples from the same batch to calculate within-batch variation, within-batch precision and within-batch accuracy. For inter-batch assessment, we analyzed three different batches to determine between-batch variation, between-batch precision and between-batch accuracy. Precision was expressed as relative standard deviation (%RSD).

Prior to conducting enzyme kinetic analysis, we first established standard curves for NESF and NEUF in PBS: acetonitrile (1:1) using LC-FD. As shown in Fig. S25, both NESF (0-20 μM) and NEUF (0-10 μM) exhibited excellent linear relationships between peak area and concentration, with linear equations of Y=5,050,488*X+1,077,374 (R^2>0.99) and Y = 13,128*X+2,033.1 (R^2>0.99), respectively. We determined the limit of detection (LOD) and limit of quantification (LOQ) for the product NEUF.

We established an analytical method using LC-FD to characterize NESF, NEUF standards, and the metabolism of NESF in recombinant human CYP3A4 (Fig.S23). These results further confirmed that NESF is metabolized by CYP3A4 to its sulfoxidized product. Since the linear response of the fluorescence intensity of the metabolic product to enzyme concentration and reaction time is crucial for enzyme activity determination, we investigated the relationship between NESF metabolite formation and both CYP3A4 concentration and incubation time. The metabolite peak area showed an excellent linear correlation with CYP3A4 concentration (0-16 nM), with the fluorescence intensity increasing linearly with enzyme concentration (linear equation: Y=384.6*X+94.807, R^2=0.998) (Fig. S24). Similarly, Fig. S25 demonstrated a linear increase in metabolite peak area over time (0-60 min). These results indicate that the generation of NESF metabolite is both CYP3A4 concentration-dependent and time-dependent.

5.DFT calculations

In this work, DFT calculations were employed to investigate the luminescence mechanisms.Ground-state structural optimizations were performed using the hybrid B3LYP functionals,[2] while the CAM-B3LYP functionals was adopted for excited-state calculations. The 6-31G** basis set was used all elements. All calculations are performed with the Gaussian 16 package.[3]

6.Molecular docking simulation

To investigate the microscopic mechanism of NESF's selectivity for CYP3A4, we analyzed the binding trajectories and binding energies of NESF with CYP3A4. The initial coordinates for the simulation structure were obtained from the Protein Data Bank: PDB code

3NXU corresponds to CYP3A4, with crystallization water and small molecules removed. NESF was docked to CYP3A4 using AutoDock Vina (version 1.1.2). A grid box of 70×70×70 $Å^3$ with a spacing of 0.375 Å was generated to encompass the catalytic pocket. Other parameters were set to default values. The system was solvated in a cubic box using the TIP3P water model, with a distance of 10 Å between the box edge and the protein.[4] Chloride ions were added to neutralize the system charge. The protein and ligand were parameterized using the CHARMM36 all-atom force field and Merck Molecular Force Field (MMFF) parameters, respectively.[5] The system energy was minimized using the steepest descent algorithm for up to 50,000 steps.[6] The LINCS constraint algorithm was employed to equilibrate the solvent and ions in the NVT and NPT ensembles.[7] A leapfrog integrator with a time step of 2 fs was used. Additionally, we utilized Discovery Studio 2016 for the 2D interaction analysis between NESF and CYP3A4. The binding energy was decomposed into van der Waals forces, electrostatic interactions, polar solvation energy, and nonpolar solvation energy.

The catalytic active center of CYP3A4 contains a heme prosthetic group with a central iron ion (Fe). In the resting state, Fe^{3+} coordinates with a water molecule, adopting a low-spin state. Upon substrate entry into the active pocket, the water molecule is displaced, and Fe^{3+} transitions to a high-spin state (remaining trivalent), facilitating subsequent electron transfer. The reduction and oxygen activation processes then occur: Fe^{3+} accepts the first electron to be reduced to Fe^{2+}. Molecular oxygen (O_2) binds to form a Fe^{2+}-O_2 complex.

7. Cytotoxicity assays and cellular fluorescence imaging

Human HepRG cells in good growth condition were harvested, and a cell suspension was prepared. The cell suspension was counted and seeded into a 96-well plate at a density of 1×10^4 cells per well. The cells were cultured overnight in an incubator. After 24 hours, when the cells had adhered well and their state had recovered, the original culture medium was discarded. A series of drug-containing culture media with final concentrations of NESF and NEUF (0, 0.01, 0.1, 0.6, 0.8, 1, 6, 8, 10, and 20 μM) were added to continue culturing for another 24 hours. The drug-containing culture media were then removed, and 100 μL of (2-methoxy-4-nitrophenyl)-3-(4-nitrophenyl)-5-(2,4-disulfophenyl)-2H-tetrazolium monosodium salt (CCK8) dilution solution (the CCK8 stock solution was diluted 10 times with the basic culture medium) was added to each well. The cells were cultured for another 2 hours in the incubator. The microplate was placed in a multimode microplate reader to measure the absorbance (OD value) at 450 nm. The cell viability was calculated, and the results were plotted using GraphPad Prism 9.5 software.

Using NESF as a fluorescent substrate, the function of CYP3A4 in living HepRG cells was imaged using a fluorescence inverted microscope. HepRG cells were seeded into 20 mm culture dishes at a density of 1×10^5 cells per dish and cultured overnight at 37 ℃ in a 5% CO_2 incubator with WE complete culture medium. The medium was then replaced with WE basic culture medium. Adherent cells were incubated with NESF (20 μM) at 37 ℃ for 120 minutes, among which the substrate was co-incubated with 1 μM CYP3cide at 37 ℃ for 120 minutes. After rinsing with PBS (pH = 7.4) to remove extracellular free substrate, fluorescent images were obtained using a fluorescence inverted microscope. One milliliter of PBS was added to each well to prevent cell shrinkage and the samples were stored in the dark.

8.Preliminary screening of inhibitors and determination of IC_{50}

A high-throughput screening method for CYP3A4 inhibitors based on LC-FD was constructed using the substrate NESF to evaluate the inhibitory effects of natural products on CYP3A4. The metabolic reaction was carried out in a 200 μL incubation system containing potassium phosphate buffer (pH 7.4, 100 mM), NESF (20 μM), NADPH solution (1 mM), and 0.2 mg/ml HLM. The final volume of the system was 100 μL. After pre-incubation at 37 ℃ for 3 min, the oxidation reaction was initiated by the addition of NADPH. Each reaction mixture was incubated at 37 ℃ for 60 min, and then 200 μL of ice-cold acetonitrile was added every 15 seconds to terminate the reaction. The terminated samples were kept on ice and then centrifuged at 20000×g for 20 min at 4 ℃. The supernatant was transferred to an HPLC vial and analyzed by LC-FD to quantify the peak area of the metabolite NEUF (λex=350 nm, λem=410 nm). The residual activity was expressed as a percentage of the control without inhibitor. The reaction time and microsomal concentration used in the experiment were within the linear range. The residual activity of CYP3A4 was determined using the following formula: Residual activity (%) = (fluorescence value of the system in the presence of inhibitor) / (fluorescence value of the system in the negative control (solvent only))×100%. The data were analyzed using GraphPad Prism V9.5 (Graphpad Software Inc., La Jolla, USA).

For natural products with CYP3A4 residual activity below 25%, a series of concentration gradients (8-12 concentrations) were selected and added to the CYP3A4 inhibitory effect evaluation system to determine the half-maximal inhibitory concentration (IC_{50}) of CYP3A4. PBS, NESF, human liver microsomes, and each natural product were added to an eppendorf tube, with a final system volume of 100 μL. After pre-incubation at 37 ℃ for 3 minutes, the oxidation reaction was initiated by the addition of NADPH. Each reaction mixture was

incubated at 37 ℃ for 60 minutes, and then 200 μL of ice-cold acetonitrile was added every 15 seconds to terminate the reaction. The terminated samples were kept on ice and then centrifuged at 20000×g for 20 minutes at 4 ℃. The supernatant was transferred to an HPLC vial and analyzed by LC-FD to quantify the peak area of the metabolite NEUF (λ_{ex}=350 nm, λ_{em}=410 nm). The residual activity was calculated by comparing the fluorescence values of the inhibitor group and the blank group. The concentration of the inhibitor at which the residual activity was 50% was defined as the IC50 of the inhibitor. The IC50 was fitted using GraphPad Prism 9.5 (GraphPad Software, Inc., CA, USA).

9.Kinetic figures, table and selected spectra

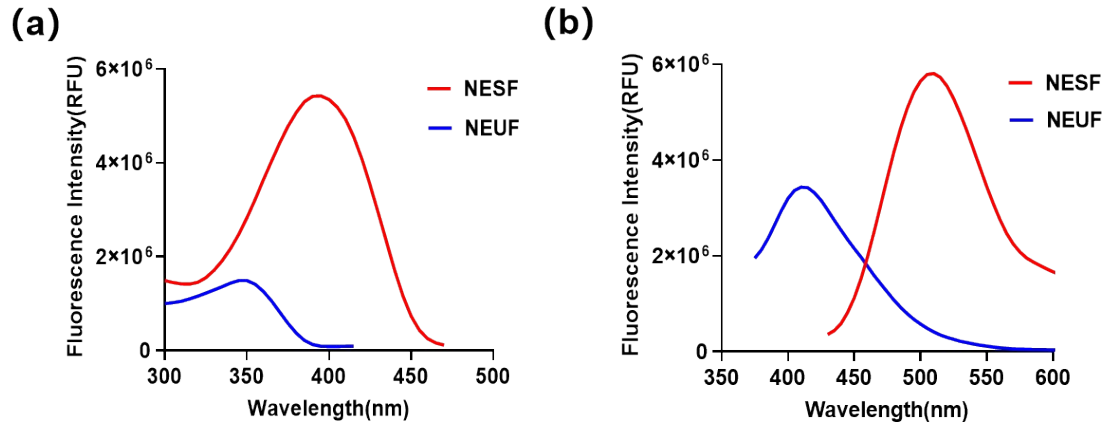

Fig.S21 (a) Absorption spectrum of NESF and its oxidative metabolite NEUF. (b) Emission spectrum of NESF and NEUF.

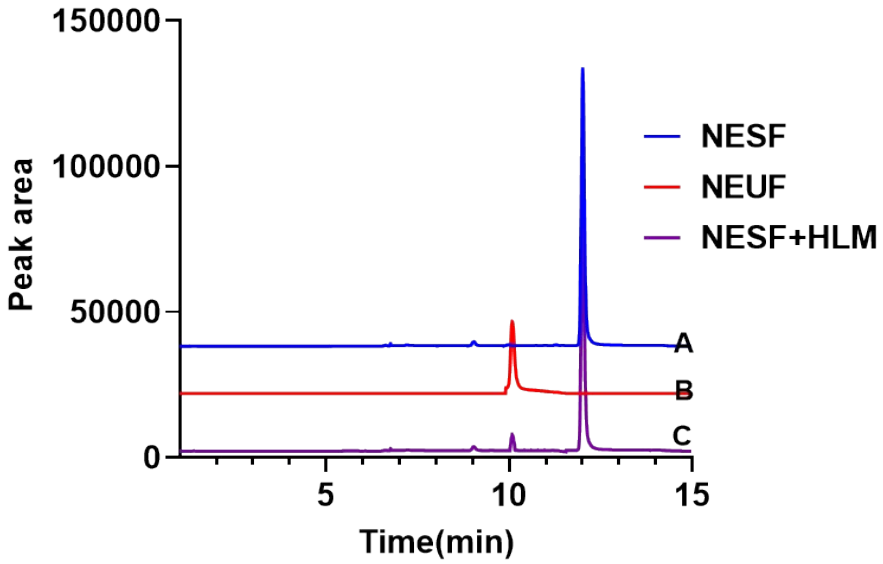

Fig S22 LC-FD chromatograms of NESF and its sulfoxidation metabolite NEUF. From top to bottom: NESF standard, NEUF standard, and NESF (20 μM) incubated with HLM (0.2 mg/mL) for 60 minutes.

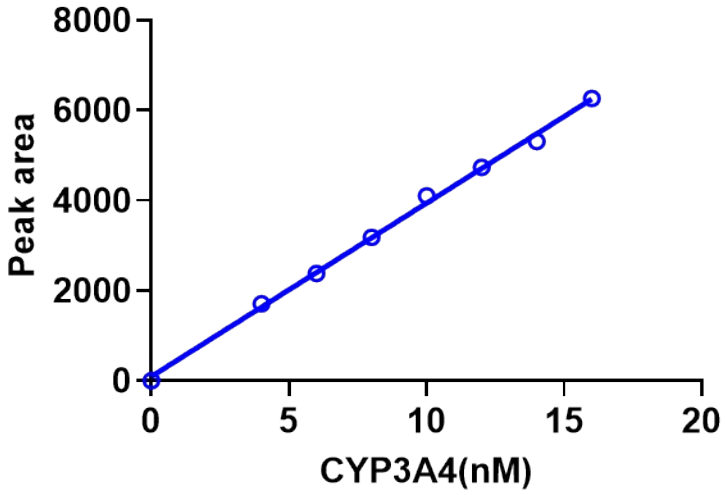

Fig S23 Linear relationship between the metabolite amount of NESF metabolized by human recombinant CYP3A4 and CYP3A4 concentration (0-16 nM). Data are presented as mean ± standard deviation (n=3).

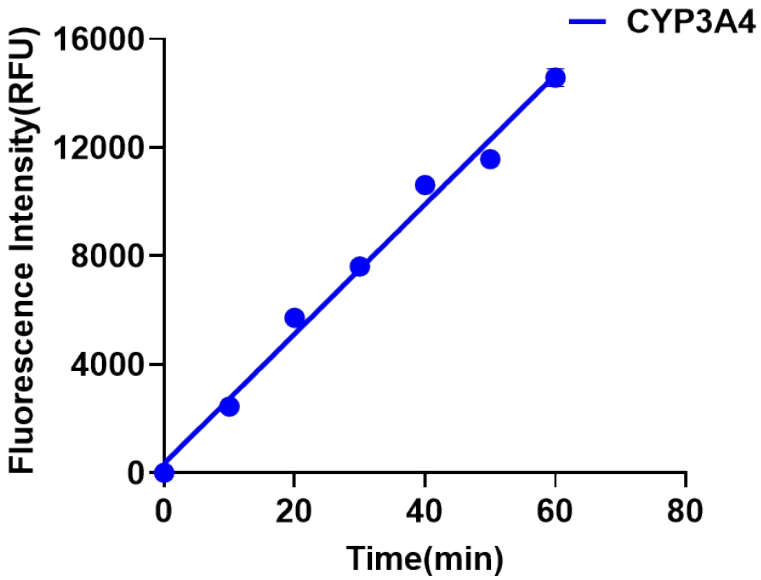

Fig S24 Linear relationship between the metabolite amount of NESF metabolized by human recombinant CYP3A4 and incubation time (0-60 min). Data are presented as mean ± standard deviation (n=3).

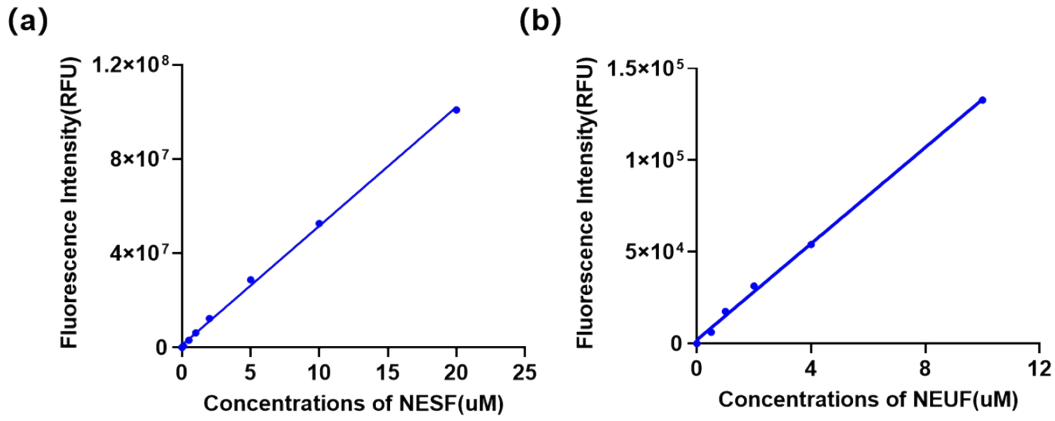

Fig S25 Standard curves of NESF(a) and NEUF(b) in PBS:acetonitrile (1:1). Data are presented as mean ± standard deviation (n=3).

Table S1 Intra-batch precision and accuracy of the method for quantitative determination of NESF.

NESF intra-assay precision and accuracy								
DUT	LLOQ 0.050 uM	accuracy (%)	LQC 0.25 uM	accuracy (%)	MQC 4 uM	accuracy (%)	HQC 15 uM	accuracy (%)
NESF	0.045	89.47%	0.26	105.65%	4.63	115.69%	14.62	97.48%
	0.044	87.16%	0.2530	101.19%	4.52	112.97%	14.72	98.14%
	0.047	94.22%	0.2172	86.88%	3.93	98.32%	17.06	113.71%
Intra-batch mean (%)	90.3%		97.9%		109.0%		103.1%	
Intra-batch SD	3.6%		9.8%		9.3%		9.2%	
Intra-batchCV (%)	4.0%		10.0%		8.6%		8.9%	
n	3		3		3		3	

Table S2 Batch-to-batch precision and accuracy of the method for quantitative determination of NESF.

NESF Batch-to-batch precision and accuracy								
DUT	LLOQ 0.050 uM	accuracy (%)	LQC 0.25 uM	accuracy (%)	MQC 4 uM	accuracy (%)	HQC 15 uM	accuracy (%)
NESF	0.045	89.47%	0.29	115.30%	4.54	113.47%	14.62	97.48%
	0.044	87.16%	0.29	115.30%	4.85	121.20%	14.72	98.14%
	0.047	94.22%	0.29	115.49%	4.31	107.83%	17.06	113.71%
	0.048	95.48%	0.27	105.65%	4.63	115.69%	16.33	108.83%
	0.043	85.53%	0.26	101.19%	4.52	112.97%	17.17	114.48%
	0.047	94.38%	0.23	86.88%	3.93	98.32%	17.01	113.37%
	0.046	91.17%	0.27	108.40%	4.68	116.89%	16.32	108.82%
	0.045	90.67%	0.27	108.25%	4.87	121.72%	16.31	108.74%
	0.045	90.56%	0.27	107.73%	4.80	120.06%	14.69	97.90%
Batch-to-batch mean(%)	91.0%		107.1%		114.2%		106.8%	
Batch-to-batch SD(%)	3.3%		9.0%		7.5%		7.1%	
Batch-to-batch CV (%)	3.7%		8.4%		6.5%		6.6%	
n	9		9		9		9	

Table S3 Intra-batch precision and accuracy of the method for quantitative determination of NEUF.

NEUF intra-assay precision and accuracy								
DUT	LLOQ 0.500 uM	accuracy (%)	LQC 1.50 uM	accuracy (%)	MQC 6 uM	accuracy (%)	HQC 9 uM	accuracy (%)
NEUF	0.42	84.16%	1.53	101.68%	6.27	104.57%	9.16	101.74%
	0.41	81.52%	1.52	101.16%	6.42	107.07%	8.91	98.95%
	0.45	89.65%	1.56	104.01%	6.34	105.68%	9.16	101.74%
Intra-batch mean (%)	85.1%		102.3%		105.8%		100.8%	
Intra-batch SD	4.1%		1.5%		1.3%		1.6%	
Intra-batch CV (%)	4.9%		1.5%		1.2%		1.6%	

n	3	3	3	3

Table S4 Batch-to-batch precision and accuracy of the method for quantitative determination of NEUF.

NEUF Batch-to-batch precision and accuracy								
DUT	LLOQ 0.500 uM	accuracy (%)	LQC 1.50 uM	accuracy (%)	MQC 6 uM	accuracy (%)	HQC 9 uM	accuracy (%)
NEUF	0.42	84.16%	1.65	109.67%	6.27	104.57%	9.16	101.74%
	0.41	81.52%	1.79	119.67%	6.42	107.07%	8.91	98.95%
	0.45	89.65%	1.73	115.43%	6.34	105.68%	9.16	101.74%
	0.47	93.92%	1.53	101.68%	5.86	97.61%	8.37	92.96%
	0.43	86.12%	1.52	101.16%	5.93	98.77%	8.53	94.79%
	0.47	93.73%	1.56	104.01%	5.62	93.73%	8.23	91.39%
	0.42	83.83%	1.57	104.85%	6.13	102.17%	8.41	93.47%
	0.44	87.29%	1.61	107.09%	5.96	99.41%	7.91	87.83%
	0.41	82.32%	1.65	109.94%	6.32	105.34%	8.37	92.95%
Batch-to-batch mean(%)	86.9%		108.2%		101.6%		95.1%	
Batch-to-batch SD(%)	4.6%		6.2%		4.5%		4.8%	
Batch-to-batch CV (%)	5.3%		5.8%		4.4%		5.0%	
n	9		9		9		9	

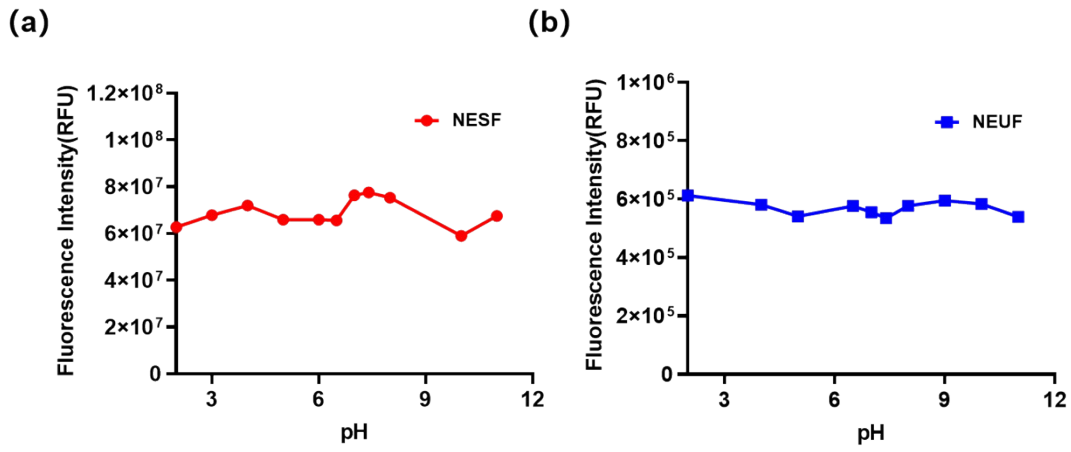

Fig S26 Effect of pH on the fluorescence intensity of NESF and its sulfoxidation metabolite

NEUF (20 μM). Different pH values were adjusted using hydrochloric acid and sodium hydroxide. Data are presented as mean ± standard deviation (n=3).

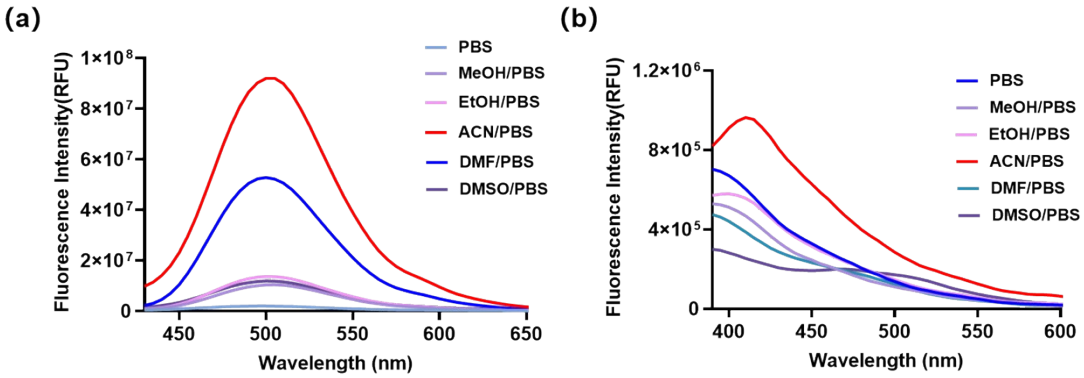

Fig S27 Effect of different solvents on the fluorescence intensity of NESF and its sulfoxidation metabolite NEUF (20 μM). Data are presented as mean ± standard deviation (n=3).

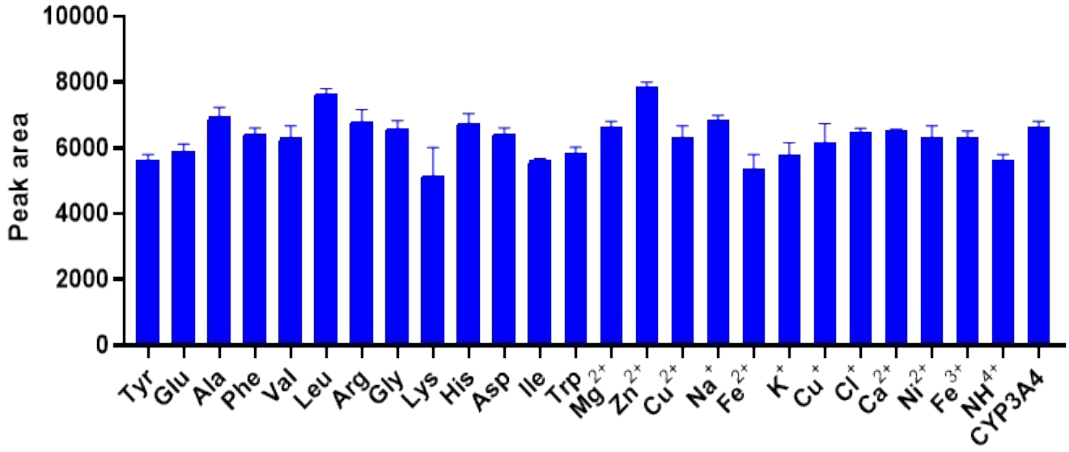

Fig S28 Product formation of NESF (20 μM) after incubation with various analytes in the CYP3A4 reaction system at 37 ℃ for 60 minutes. Data are presented as mean ± standard deviation (n=3).

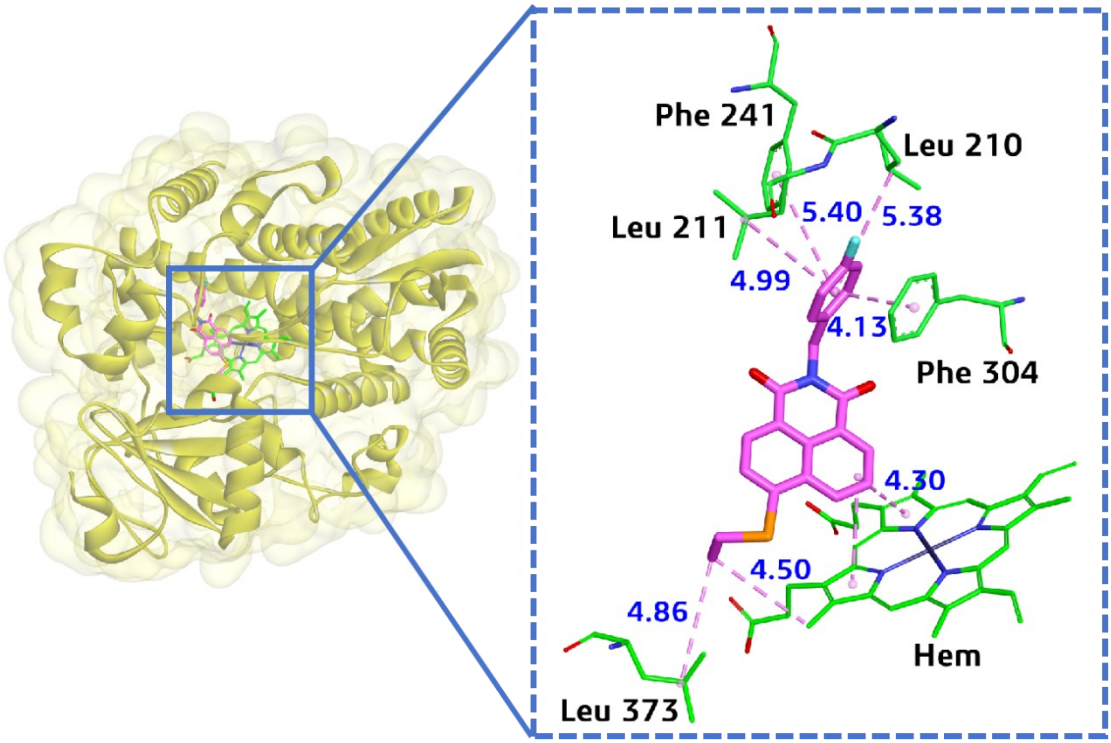

Fig.S29 The binding conformation of NESF in hCYP3A4 obtained from equilibrium trajectory. The PDB ID of the initial conformation is 3NXU.

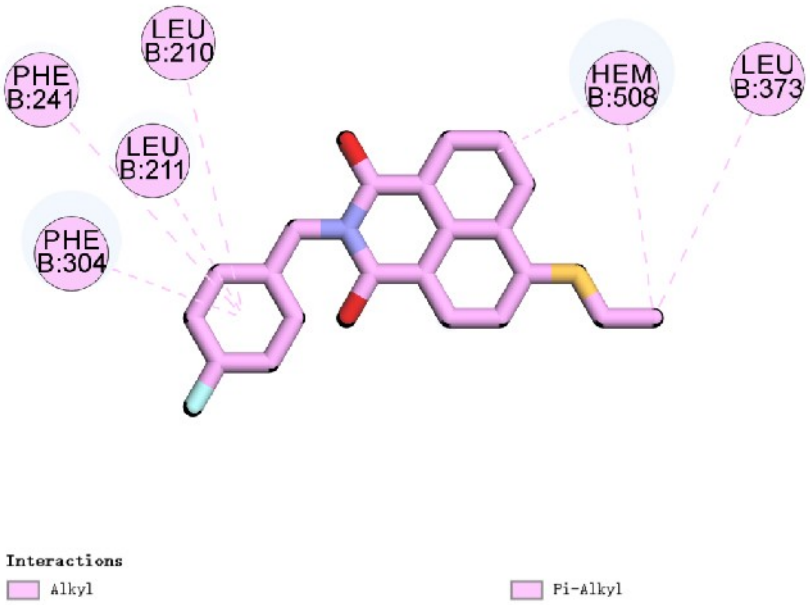

Fig S30 2D interaction analysis of NESF with CYP3A4.

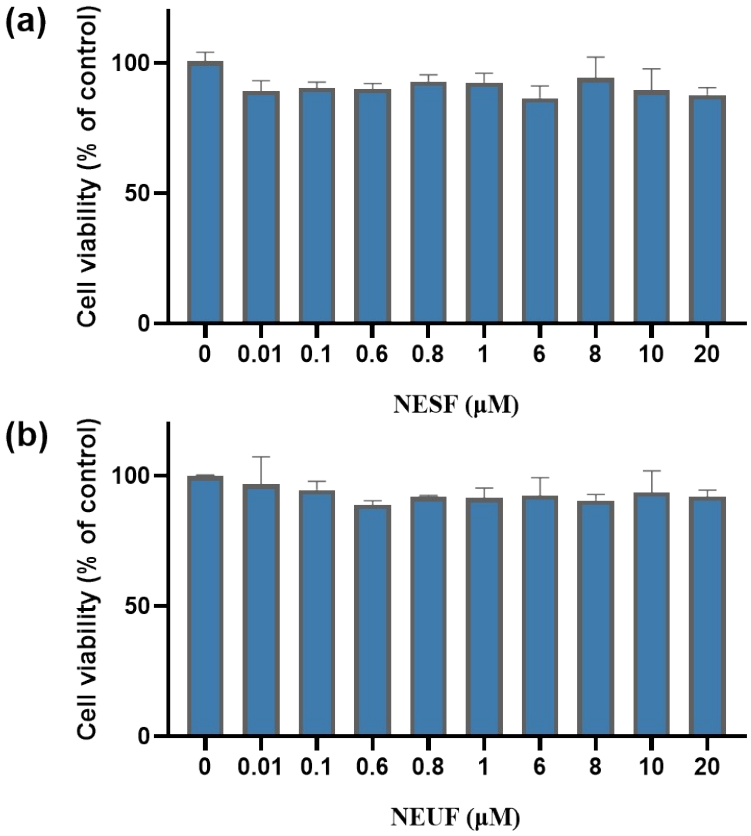

Fig S31 Cytotoxicity assay.

Table S5 Inhibitory effects of 104 natural products on CYP3A4.

No.	Compound name	CAS	Residual activity (%) *
a-1	Anthraquinone	84-65-1	107.38
a-2	1,4-Anthraquinone	635-12-1	14.03
a-3	1-Hydroxyanthraquinone	129-43-1	37.55
a-4	1-Amino anthraquinone	82-45-1	59.78
a-5	1,8-Dihydroxyanthraquinone	117-10-2	35.02
a-6	1,8-Dichloroanthraquinone	82-43-9	105.58
a-7	Alizarin	72-48-0	52.52
a-8	Alizarin Red	130-22-3	34.59
a-9	Chrysophanic acid	481-74-3	45.73
a-10	Rhein	478-43-3	49.52
a-11	Emodin	518-82-1	24.16

No.	Compound name	CAS	Residual activity (%) *
a-12	Physcione	521-61-9	64.09
a-13	Vat Blue 4	81-77-6	61.61
b-1	1,4-Dihydroxyanthraquinone	81-64-1	33.36
b-2	Solvent Violet 13	81-48-1	40.55
b-3	1,5-Diamino-4,8-dihydroxyanthraquinone	145-49-3	24.84
b-4	2-Methylanthraquinone	84-54-8	38.30
b-5	2-Ethyl anthraquinone	84-51-5	44.34
b-6	2-Chloroanthracene-9,10-dione	131-09-9	48.97
b-7	Anthraquinone-2-carboxylic acid	117-78-2	29.29
b-8	2,6-Dihydroxyanthraquinone	84-60-6	29.09
b-9	2,6-Dibromoanthraquinone	633-70-5	13.35
b-10	Sennoside A	81-27-6	31.88
b-11	Sennoside B	128-57-4	30.40
b-12	Alizarin Complexone	3952-78-1	24.05
b-13	2-Bromoanthraquinone	572-83-8	16.59
c-1	1,5-Dihydroxyanthraquinone	117-12-4	44.64
c-2	Quercetin	117-39-5	20.18
c-3	Lupeol	545-47-1	33.74
c-4	Panaxadiol	19666-76-3	84.43
c-5	Maslinic acid	4373-41-5	68.37
c-6	β-Boswellic Acid	631-69-6	47.08
c-7	Oleanolic acid	508-02-1	59.34
c-8	Asiatic acid	464-92-6	41.66
c-9	Panaxatriol	32791-84-7	52.70
c-10	Ursolic acid	77-52-1	51.01
c-11	Hederagenin	465-99-6	25.16
c-12	Betulinic acid	472-15-1	16.91
c-13	Bilobetin	552.48	20.55

No.	Compound name	CAS	Residual activity (%) *
d-1	Celastrol	34157-83-0	41.72
d-2	Ganoderic acid B	81907-61-1	56.19
d-3	Friedelin	559-74-0	54.31
d-4	Alpha-boswellic acid	471-66-9	109.39
d-5	Pachymic acid	29070-92-6	18.91
d-6	Protopanaxadiol	30636-90-9	33.60
d-7	Acetyl-11-keto-β-boswellic acid	17019-92-0	22.67
d-8	Polygalacic acid	22338-71-2	15.71
d-9	Glycyrrhetinic Acid	471-53-4	53.50
d-10	Betulin	559-70-6	17.44
d-11	Regelide	84104-71-2	15.32
d-12	Glycyrrhizic acid	1405-86-3	52.68
d-13	Ziyuglycoside II	35286-59-0	87.52
e-1	Betulinicaldehyde	13159-28-9	80.13
e-2	23-Hydroxybetulinic acid	85999-40-2	105.55
e-3	Betulinic acid	472-15-1	41.02
e-4	Echinocystic acid	510-30-5	56.30
e-5	Sciadopitysin	521-34-6	55.36
e-6	MudanpiosideC	172760-03-1	16.92
e-7	Chlorogenic acid	327-97-9	36.25
e-8	Corosolic acid	4547-24-4	61.08
e-9	Hederagenin	465-99-6	21.91
e-10	Palmatine	3486-67-7	35.06
e-11	Asiatic acid	464-92-6	107.30
e-12	Astragalin	480-10-4	86.41
e-13	Paris Saponin VII	68124-04-9	33.21
f-1	Paeoniflorin	23180-57-6	30.97
f-2	Polyphyllin I	50773-41-6	74.23

No.	Compound name	CAS	Residual activity (%) *
f-3	Polyphyllin II	50773-42-7	16.80
f-4	Icariside II	113558-15-9	82.38
f-5	Daidzein	486-66-8	69.99
f-6	Hesperetin	69097-99-0	44.08
f-7	Isoflavone	574-12-9	41.34
f-8	Neobavaisoflavone	41060-15-5	15.33
f-9	Puerarin	3681-99-0	26.89
f-10	Nobiletin	478-01-3	41.57
f-11	Myricetin	529-44-2	30.63
f-12	Cyanidin Chloride	528-58-5	26.33
f-13	Glycitein	40957-83-3	30.56
g-1	Kaempferol	520-18-3	31.32
g-2	Taxifolin	480-18-2	27.61
g-3	Bavachin	19879-32-4	26.79
g-4	Farrerol	24211-30-1	11.74
g-5	Biochanin A	491-80-5	31.89
g-6	Dihydrokaempferol	480-20-6	24.73
g-7	Formononetin	485-72-3	38.56
g-8	Ipriflavone	35212-22-7	31.56
g-9	Cynaroside	5373-11-5	48.38
g-10	Chrysin	480-40-0	32.07
g-11	Luteolin	491-70-3	19.24
g-12	3,6-Dihydroxyflavone	108238-41-1	81.35
g-13	6-HYDROXYFLAVONE	6665-83-4	42.01
h-1	Neoliquiritin	5088-75-5	106.04
h-2	Acacetin	480-44-4	34.99
h-3	Isoxanthohumol	521-48-2	81.43
h-4	7,4'-Dihydroxyflavone	2196-14-7	86.86

No.	Compound name	CAS	Residual activity (%) *
h-5	Apigenin	520-36-5	47.21
h-6	Diosmetin	520-34-3	14.17
h-7	3',4'-Dihydroxyflavone	4143-64-0	24.28
h-8	Daidzein	486-66-8	35.48
h-9	Glycitin	40246-10-4	29.33
h-10	Cynaroside	5373-11-5	29.52
h-11	5-Hydroxyflavone	491-78-1	18.79
h-12	Isoginkgetin	548-19-6	28.96
h-13	Amentoflavone	1617-53-4	15.43

The final concentration of each test inhibitor was 5 μM, and the residual activity was expressed as the mean value of triplicate measurements.

10. References

1 (a)E. Tseng, R. L. Walsky, R. A. Luzietti, J. J. Harris, R. E. Kosa, T. C. Goosen, M. A. Zientek and R. S. Obach, Drug Metabolism and Disposition, 2014, 42, 1163–1173.(b)T. D. Bjornsson, J. T. Callaghan, H. J. Einolf, V. Fischer, L. Gan, S. Grimm, J. Kao, S. P. King, G. Miwa, L. Ni, G. Kumar, J. McLeod, R. S. Obach, S. Roberts, A. Roe, A. Shah, F. Snikeris, J. T. Sullivan, D. Tweedie, J. M. Vega, J. Walsh, S. A. Wrighton, Drug Metab Dispos, 2003, 31, 815–832.(c)R. L. Walsky, R. S. Obach, E. A. Gaman, J.-P. R. Gleeson and W. R. Proctor, Drug Metab Dispos, 2005, 33, 413–418.(d)W. Zhang, T. Kilicarslan, R. F. Tyndale and E. M. Sellers, Drug Metab Dispos, 2001, 29, 897–902.(e)J. M. Rae, N. V. Soukhova, D. A. Flockhart and Z. Desta, Drug Metab Dispos, 2002, 30, 525–530.(f)Y.-K. Wang, X.-N. Yang, W.-Q. Liang, Y. Xiao, Q. Zhao, X.-R. Xiao, F. J. Gonzalez and F. Li, Xenobiotica, 2019, 49, 655–670.

2 (a)C. Jean‐Louis, Int J Quantum Chem, 1993, 47: 101. (b)K. Burke, J Chem Phys, 2012, 136: 150901.

3 M. J. Frisch, G. W. Trucks, H. B. Schlegel, G. E. Scuseria, M. A. Robb, J. R. Cheeseman, G. Scalmani, V. Barone, G. A. Petersson, H. Nakatsuji, X. Li, M. Caricato, A. V. Marenich, J. Bloino, B. G. Janesko, R. Gomperts, B. Mennucci, H. P. Hratchian, J. V. Ortiz, A. F. Izmaylov, J. L. Sonnenberg, D. Williams-Young, F. Ding, F. Lipparini, F. Egidi, J. Goings, B. Peng, A. Petrone, T. Henderson, D. Ranasinghe, V. G. Zakrzewski, J. Gao, N. Rega, G. Zheng, W. Liang, M. Hada, M. Ehara, K. Toyota, R. Fukuda, J. Hasegawa, M. Ishida, T. Nakajima, Y. Honda, O. Kitao, H. Nakai, T. Vreven, K. Throssell, J. A. Montgomery, Jr., J. E. Peralta, F. Ogliaro, M. J. Bearpark, J. J. Heyd, E. N. Brothers, K. N. Kudin, V. N. Staroverov, T. A. Keith, R. Kobayashi, J. Normand, K. Raghavachari, A. P. Rendell, J. C. Burant, S. S. Iyengar, J. Tomasi, M. Cossi, J. M. Millam, M. Klene, C. Adamo, R. Cammi, J.

W. Ochterski, R. L. Martin, K. Morokuma, O. Farkas, J. B. Foresman, and D. J. Fox, Gaussian 16, Revision A.03: Gaussian, Inc., Wallingford CT, 2016.

4 W. L. Jorgensen, J. Chandrasekhar, J. D.Madura, R. W. Impey, M. L.Klein, J Chem Phys, 1983, 79: 926-935.

5 (a)K. Vanommeslaeghe, E. Hatcher, C. Acharya, S. Kundu, S. Zhong, J. Shim, E. Darian, O. Guvench, P. Lopes, I. Vorobyov and A. D. Mackerell, J Comput Chem, 2010, 31, 671 – 690. (b)V. Zoete, M. A. Cuendet, A. Grosdidier and O. Michielin, J Comput Chem, 2011, 32, 2359 – 2368.

6 T. A. Darden, D. M. York, L. G. Pedersen, J Chem Phys, 1993, 98, 10089-10092.

7 B. Hess, H.Bekker, H. J. C. Berendsen, J. G. E. M. Fraaije, J Comput Chem, 1997, 18: 1463-1472.

8 (a)R. Kumari, R. Kumar, J Chem Inf Model, 2014, 54, 1951 – 1962. (b) N. A. Baker, D. Sept, S. Joseph, M. J. Holst and J. A. McCammon, Proc. Natl. Acad. Sci. U.S.A., 2001, 98, 10037 – 10041.